The Journal of the Astronautical Sciences (2020) 67:1470–1499
https://doi.org/10.1007/s40295-020-00233-0

ORIGINAL ARTICLE

Autonomous Precision Control of Satellite Formation Flight under Unknown Time-Varying Model and Environmental Uncertainties

Hancheol Cho[1] · Firdaus E. Udwadia[2] · Thanapat Wanichanon[3]

Published online: 15 October 2020

Abstract

This paper presents a new methodology for autonomous precision control of satellite formations in the presence of uncertainties and external disturbances. The methodology is developed in two steps. First, using a nominal system model that provides the best assessment of real-life uncertainties, a nonlinear controller that satisfies the formation configuration requirements is developed without making any linearizations/approximations. This closed-form control strategy is inspired by results from analytical dynamics and uses the fundamental equation of constrained motion. In the second step, an adaptive continuous robust controller is developed to compensate for model uncertainties and field disturbances to which the satellite formation may be subjected. This controller is based on a generalization of the concept of sliding mode control, and produces no chattering. The control gain is automatically updated in real time and the norm of the trajectory error is guaranteed to lie within user-provided desired bounds without a priori knowledge of the uncertainty/disturbance bounds. Since the control force is explicitly obtained, the approach is not computationally intensive, thereby making the approach ideal for on-orbit autonomous real-time satellite formation control. Numerical simulations demonstrate the effectiveness of the proposed control methodology, in which a desired formation configuration is required to be precisely and autonomously maintained despite large initial trajectory errors in the presence of uncertain satellite mass and environmental disturbances.

Keywords Satellite formation flying · Time-varying uncertainties in flight environment and satellite model · Unknown uncertainty bounds · Autonomous real-time precision control · Fundamental equation of constrained motion · Lyapunov stability

✉ Hancheol Cho
hancheol.cho@gmail.com

Extended author information available on the last page of the article

Introduction

Satellite formation flying (SFF) has been in the spotlight for the last two decades because the use of multiple small satellites offers advantages such as high-resolution imaging and enhanced flexibility, efficiency, and economic benefits compared with a single large satellite [1]. However, more advanced technology is required for precision formation control mainly due to coupled dynamics between the distributed satellites and severe system uncertainties/disturbances, i.e., nonuniform gravitational potential, atmospheric drag, solar radiation pressure, and luni-solar perturbations.

The SFF problem is usually explored using unperturbed, linearized equations of the real nonlinear dynamics such as Clohessy-Wiltshire equations [2] for a circular reference orbit or Tschauner-Hempel equations [3] for an elliptical reference orbit. However, controllers designed based on these linearized dynamics must compensate for the uncertain effects of various perturbations in order to be used in a real-world SFF mission. Over the last few decades, numerous robust control strategies have been developed and proposed. Won and Ahn [4] developed nonlinear dynamic equations of relative motion for a constant distance separation between satellites and utilized the state-dependent Riccati equation technique to control the satellites modeled by the newly developed relative equations. Two cases were exemplified under the effects of J_2 oblateness, atmospheric drag, and solar radiation pressure: noncircular and noncoplanar Molniya orbit formation flying and constant angle separation formation flying in the same orbital plane. Wong et al. [5] proposed an adaptive output feedback control for relative position tracking. The lack of velocity measurements was assumed and estimated through a high-pass filter and a parameter adaptation control law was constructed to ensure semi-global, asymptotic stability of the tracking error in the presence of constant disturbance forces. In de Queiroz et al. [6] a Lyapunov-based, adaptive control law was developed to guarantee global asymptotic convergence of the relative position tracking error in the presence of unknown, constant or slowly-varying uncertainties. Vignal and Pernicka [7] used a state-feedback linearization technique for satellite formation control in the presence of the Earth oblateness and measurement noise assuming limited on-off thrusting capabilities. Breger and How [8] presented a variant of the Gauss's variational equations that incorporates the effects of J_2 and developed an online, optimization-based, model predictive controller in an effort to improve robustness against model uncertainties. It was shown that fuel efficiency was increased and many types of constraints could be handled such as error-box maintenance. Using eccentricity/inclination vector representation, Lim et al. [9] was able to design a robust model predictive controller in the face of model uncertainties or external disturbances while satisfying various input and/or state constraints and avoiding collision risk. However, the maximum bound on the uncertainties was required to be known for the elimination of the uncertainty effects. Hu and Ng [10] proposed a robust control scheme for two spacecraft in formation subjected to time-varying disturbances based on sliding mode control. They also assumed that the disturbances are bounded by a positive scalar function which is a priori known.

Amidst others, sliding mode control (SMC) [11, 12] has attracted much attention for powerful robustness to matched uncertainties and external disturbances, computational simplicity, fast response, and easy implementation. Yeh et al. [13] developed discontinuous control laws based on SMC assuming that the maximum magnitude of the

uncertainties imposed on the SFF dynamics is a priori known. Conventional SMC methods in general endeavor to place the system trajectories onto the so-called sliding surface and are usually characterized by discontinuous control and high control gains. In order to prevent this so-called chattering problem resulting from the use of discontinuous control action, which is usually pointed out as the main drawback of SMC, the boundary-layer approach [14] was introduced. However, since the boundary layer approach generally introduces a loss of accuracy due to its continuous approximation, three different approaches for continuous SMC were proposed by Massey and Shtessel [15], which include SMC augmented with a sliding mode disturbance observer, a super-twisting algorithm, and integral SMC. Udwadia et al. [16] used various kinds of continuous functions to effectively control relative motion without chattering. Although they do not exactly converge to zero, the errors are guaranteed to be made arbitrarily small. However, in Massey and Shtessel [15] and Udwadia et al. [16] a good estimate of the upper bound for the uncertainties is assumed to be available, something that might often be quite difficult to obtain in practice. Another practical limitation is that the control input saturation is not considered. Godard [17] introduced adaptive fault-tolerant control laws based on SMC in the presence of uncertain satellite mass and unknown disturbances. In their approach exact knowledge of the uncertain mass or the magnitude of the disturbances is not necessary and two different sliding surfaces (conventional SMC and nonsingular terminal SMC) are designed and compared. Bae and Kim [18] proposed an adaptive SMC strategy to include the cases when the upper bounds on the modeling errors or external disturbances are unknown. The uncertainties were also estimated using neural networks to save control effort and reduce chattering. However, they assumed zero initial errors. This assumption is important, because without it, robustness of SMC is not guaranteed until the system arrives at the sliding surface. In the approach presented herein this assumption is not necessary.

In this paper, a two-step adaptive control methodology for precision satellite formation control is proposed by generalizing the notion of SMC in the presence of model uncertainties and uncertain space environments. It is assumed that the magnitude of the uncertainties is unknown but bounded. The first step considers the nonlinear 'nominal' satellite formation system, which is defined as a deterministic system that includes our best estimates—based on theory/experiments/intuition and/or experience—of the uncertain parameters. An explicit real-time on-orbit controller is obtained through the use of the fundamental equation of constrained motion [19]. This controller causes the nominal system to precisely track a user-specified desired trajectory and it considers the nonlinear system in its entirety without any linearizations/approximations. This approach has been successfully applied to modeling and control of complex multi-body dynamical systems [20–26] and satellite formation systems [27–30]. An initial misalignment problem is also resolved by introducing a second-order damped system, guaranteeing the asymptotic stability of a constrained SFF system. In the second step, an adaptive control methodology is developed for on-orbit real time precision tracking of the uncertain system in which knowledge of the values of the upper bounds on the uncertainties in the system is not required. This controller updates its gain in an autonomous manner to cancel out the effects of all the uncertainties not considered in the first step of the control methodology *without requiring any knowledge of the bound on these uncertainties*. Also, it produces no chattering because only continuous functions are involved and it successfully tracks the nominal trajectory generated by the

controller developed in the first step despite the presence of uncertainties in the satellite's properties (its mass) and unknown disturbances. Since initial errors have been already considered when generating the nominal trajectory in the first step, the sliding variable starts with zero and the sliding mode begins from the initial time regardless of the values of the initial trajectory errors. This greatly enhances the performance of the control methodology proposed herein and provides a significant advance over available approaches in the current literature.

The structure of the paper is as follows. In Section 2 a satellite formation flight model is presented for which the equations of motion are obtained. Next, the two-step control methodology is briefly presented for precision trajectory control of the formation in which both the mass of the satellite and the external disturbances are uncertain. Section 3 deals with the first step in this two-step approach using the fundamental equation of constrained motion and assuming the nominal satellite formation system with no uncertainties. Section 4 deals with the development of an adaptive control methodology based on continuous SMC techniques. As a prelude, Subsection 4.1 first considers the development of a precision tracking control approach in which knowledge of the uncertainty bounds is needed. This subsection serves as a contrast to, and a jumping point for, the adaptive control approach developed in Subsection 4.2 that follows in which no knowledge of the uncertainty bounds on the mass of the satellite and the external environmental disturbances is needed. In this subsection we provide the theoretical underpinnings of our approach for controlling the satellite formation in the presence of uncertainties while guaranteeing the satisfaction of a user-specified bound, however small, on the tracking error. Section 5 provides numerical simulations of the approach when applied to the equations of motion given in Section 2. These in-depth simulations include studies on the effects of limitations on the thrust force on the effectiveness of the proposed control methodology. They show the ease and accuracy with which on-orbit real-time precision tracking of uncertain systems can be accomplished. Section 6 gives the conclusions.

Satellite Formation Flight Model and Equations of Motion

The proposed formation flight model comprises a leader satellite which orbits the Earth in a general elliptical planar trajectory and a follower satellite that moves relative to the leader satellite in a desired configuration. It is assumed that we only focus on controlling the follower satellite to move along the desired relative reference trajectory around the leader satellite that is separately controlled to follow a predetermined elliptical orbit. In this paper, the relative motion is described in the so-called local-vertical, local-horizontal (LVLH) frame [31] fixed at the mass center of the leader satellite, where the x-axis is directed radially outward along the local vertical, the z-axis is along the orbital angular momentum vector of the leader satellite, and the y-axis completes the right-handed triad. In this frame the nonlinear equations of relative motion for the follower satellite, considering the control thrust and external disturbance forces, can be written in the following form [32]:

$$m\ddot{\boldsymbol{q}} = m\begin{bmatrix}\ddot{x}\\ \ddot{y}\\ \ddot{z}\end{bmatrix} = m\begin{bmatrix}0 & 2\dot{\theta} & 0\\ -2\dot{\theta} & 0 & 0\\ 0 & 0 & 0\end{bmatrix}\begin{bmatrix}\dot{x}\\ \dot{y}\\ \dot{z}\end{bmatrix} + m\begin{bmatrix}\theta^2 & \ddot{\theta} & 0\\ -\ddot{\theta} & \theta^2 & 0\\ 0 & 0 & 0\end{bmatrix}\begin{bmatrix}x\\ y\\ z\end{bmatrix} - \frac{m\mu_{\oplus}}{\left[(x+r_L)^2+y^2+z^2\right]^{3/2}}\begin{bmatrix}x+r_L\\ y\\ z\end{bmatrix} + \begin{bmatrix}\frac{m\mu_{\oplus}}{r_L^2}\\ 0\\ 0\end{bmatrix} + \begin{bmatrix}U_x\\ U_y\\ U_z\end{bmatrix} + \begin{bmatrix}D_x\\ D_y\\ D_z\end{bmatrix} \tag{1}$$

where m is the *unknown* time-varying mass of the follower satellite, $\boldsymbol{q} = [x\ y\ z]^T$ is the position vector in the LVLH frame of the follower satellite where the superscript 'T' denotes the transpose of a vector or a matrix, the dot denotes the time derivative of a variable, θ refers to the true argument of latitude (sum of the argument of periapsis and true anomaly), r_L is the distance from the center of the Earth to the mass center of the leader satellite, and $\mu_{\oplus}$ is the gravitational parameter of the Earth. Also, U_i $(i = x, y, z)$ denotes the control thrust input vector of the follower satellite in each direction of the LVLH frame and D_i is an element of the *unknown* net disturbance forces caused by nonuniform gravitational potential, atmospheric drag, and so on. Furthermore, the mass of the follower, $m(t) > 0$, is assumed to be time-varying and its rate of change, $\dot{m}$, is related to the control thrust vector via the relation [33]

$$\dot{m} = -\lambda\|\boldsymbol{U}\|, \tag{2}$$

where $\lambda = \frac{1}{I_{sp}g_0} > 0$, where I_{sp} the specific impulse, g_0 is the acceleration due to gravity at sea level, $\boldsymbol{U}(t) = [\,U_x \quad U_y \quad U_z\,]^T$ is the control thrust vector, and $\|\cdot\|$ denotes the Euclidean norm of a vector. In this paper, assuming an I_{sp} value of 1280 s, $\lambda = 8.0 \times 10^{-5}$ s/m is used, assuming that a Hall thruster system is used for propulsion [34].In the present investigation, the projected circular formation [35] is taken as the desired formation configuration. In this formation the relative distance between the leader and the follower satellites is maintained constant when the relative trajectory is projected onto the y-z plane of the LVLH frame. Mathematically, the formation requirement is described by $y_d(t)^2 + z_d(t)^2 = \rho^2$ where ρ is a constant radius of the projected circle and the subscript 'd' is appended to denote desired quantities. Also, to achieve a bounded motion, the motion projected onto the x-z plane is constrained to lie on a straight line $2x_d(t) = z_d(t)$. More specifically, the corresponding projected circular formation equations satisfy the following desired trajectory in the LVLH frame:

$$x_d(t) = \frac{\rho}{2}\sin(nt), y_d(t) = \rho\cos(nt), z_d(t) = \rho\sin(nt). \tag{3}$$

At each instant of time the solution $\boldsymbol{q}(t)$ of Eq. (1) is required to track $\boldsymbol{q}_d(t) = [\,x_d \quad y_d \quad z_d\,]^T$, where $x_d(t)$, $y_d(t)$, and $z_d(t)$ satisfy Eq. (3).

In the next section, a model-based explicit control $\boldsymbol{U}^n(t)$ is obtained by first (i) assuming a constant nominal value (estimate), m_0, of the mass m and (ii) ignoring the disturbance force vector $\boldsymbol{D}(t) = [\,D_x \quad D_y \quad D_z\,]^T$ in Eq. (1). This system is called the 'nominal' system. It is deterministic with its equation of motion fully known.

Model-Based Control for the Nonlinear Nominal System with no Uncertainties

In this paper a two-step procedure is used in developing a controller so that the follower satellite tracks the required trajectory requirements given in Eq. (3) in spite of model uncertainties and external disturbances. This section deals with the first step in which (i) a nominal system with no uncertainties is considered, and (ii) an explicit closed-form controller for the nonlinear system is obtained using the Fundamental Equation of Constrained Motion [36]. The trajectory requirements (Eq. (3)) are viewed as constraints on the system and the resulting control that is explicitly found drives the leader-follower system to satisfy the desired formation configuration without any errors [22].

Then, the unconstrained equation of motion of the nominal system to which the control $\boldsymbol{U}^n(t)$ is applied so that it satisfies Eq. (3) is given by

$$m_0\,\ddot{\boldsymbol{q}}\,(t) = m_0 \begin{bmatrix} \ddot{x}(t) \\ \ddot{y}(t) \\ \ddot{z}(t) \end{bmatrix} = m_0 \begin{bmatrix} a_x\left(t, \boldsymbol{q}, \dot{\boldsymbol{q}}\right) \\ a_y\left(t, \boldsymbol{q}, \dot{\boldsymbol{q}}\right) \\ a_z\left(t, \boldsymbol{q}, \dot{\boldsymbol{q}}\right) \end{bmatrix} + \begin{bmatrix} U_x^n(t) \\ U_y^n(t) \\ U_z^n(t) \end{bmatrix} = m_0 \boldsymbol{a}\left(t, \boldsymbol{q}, \dot{\boldsymbol{q}}\right) + \boldsymbol{U}^n(t), \quad (4)$$

where m_0 is the nominal mass that is assumed to be known, $\boldsymbol{U}^n(t)$ is the control force applied to the nominal system ('n' for nominal), and the 'unconstrained' acceleration $\boldsymbol{a}\left(t, \boldsymbol{q}, \dot{\boldsymbol{q}}\right)$ is given by

$$\boldsymbol{a} \triangleq \begin{bmatrix} a_x \\ a_y \\ a_z \end{bmatrix} = \begin{bmatrix} 0 & 2\dot{\theta} & 0 \\ -2\dot{\theta} & 0 & 0 \\ 0 & 0 & 0 \end{bmatrix} \begin{bmatrix} \dot{x} \\ \dot{y} \\ \dot{z} \end{bmatrix} + \begin{bmatrix} \theta^2 & \ddot{\theta} & 0 \\ -\ddot{\theta} & \theta^2 & 0 \\ 0 & 0 & 0 \end{bmatrix} \begin{bmatrix} x \\ y \\ z \end{bmatrix} - \frac{\mu_\oplus}{\left[(x + r_L)^2 + y^2 + z^2\right]^{3/2}} \begin{bmatrix} x + r_L \\ y \\ z \end{bmatrix} + \begin{bmatrix} \frac{\mu_\oplus}{r_L^2} \\ 0 \\ 0 \end{bmatrix} \quad (5)$$

The controlled motion $\boldsymbol{q} = [x \quad y \quad z]^T$ which is the solution to Eq. (4) is required to satisfy the constraint equation Eq. (3) by the application of the control force vector $\boldsymbol{U}^n(t)$ such that the following constraint equation holds:

$$\boldsymbol{\Phi} = \begin{bmatrix} \phi_1 \\ \phi_2 \\ \phi_3 \end{bmatrix} = \begin{bmatrix} x - \frac{\rho}{2}\sin nt \\ y - \rho\cos nt \\ z - \rho\sin nt \end{bmatrix} = \begin{bmatrix} 0 \\ 0 \\ 0 \end{bmatrix}. \tag{6}$$

This constraint equation should be satisfied for all time, but it is more practical to assume that there are initial errors in the satisfaction of Eq. (6). Hence, we instead consider the following constraint equation obtained by Baumgarte's stabilization technique [37]:

$$\ddot{\boldsymbol{\Phi}} + \alpha\dot{\boldsymbol{\Phi}} + \beta\boldsymbol{\Phi} = \boldsymbol{0}, \tag{7}$$

where α and β are positive constants which will act as the damping coefficient and the stiffness of the second-order damped system. Then, as time goes by, the constraints in $\boldsymbol{\Phi}(t)$ will decay to zero and satisfy Eq. (6), and by properly selecting the values of α and β, one can adjust the decay rate. The system in Eq. (7) is overdamped if $\alpha^2 - 4\beta > 0$, critically damped if $\alpha^2 - 4\beta = 0$, and underdamped if $\alpha^2 - 4\beta < 0$. The augmented constraint equation, Eq. (7), can then be written in matrix form:

$$\underbrace{\begin{bmatrix} 1 & 0 & 0 \\ 0 & 1 & 0 \\ 0 & 0 & 1 \end{bmatrix}}_{\mathbf{A}} \begin{bmatrix} \ddot{x} \\ \ddot{y} \\ \ddot{z} \end{bmatrix} = \underbrace{\begin{bmatrix} -\frac{n^2\rho}{2}\sin(nt) - \alpha\left[\dot{x} - \frac{n\rho}{2}\cos(nt)\right] - \beta\left[x - \frac{\rho}{2}\sin(nt)\right] \\ -n^2\rho\cos(nt) - \alpha\left[\dot{y} + n\rho\sin(nt)\right] - \beta\left[y - \rho\cos(nt)\right] \\ -n^2\rho\sin(nt) - \alpha\left[\dot{z} - n\rho\cos(nt)\right] - \beta\left[z - \rho\sin(nt)\right] \end{bmatrix}}_{\boldsymbol{b}}, \tag{8}$$

or more succinctly as,

$$\mathbf{A}\ddot{\boldsymbol{q}} = \boldsymbol{b}, \tag{9}$$

where $\mathbf{A} = \begin{bmatrix} 1 & 0 & 0 \\ 0 & 1 & 0 \\ 0 & 0 & 1 \end{bmatrix}$, $\boldsymbol{q} = [x \quad y \quad z]^T$, and the 3 by 1 vector $\boldsymbol{b}$ is the right-hand side of Eq. (8).

Udwadia and Kalaba [36] showed that the explicit control force vector $\boldsymbol{U}^n(t)$ that renders the constraints Eq. (9) exactly satisfied and simultaneously minimizes the control cost $J = m_0\left[\ddot{\boldsymbol{q}}(t) - \boldsymbol{a}(t)\right]^T\left[\ddot{\boldsymbol{q}}(t) - \boldsymbol{a}(t)\right] = \frac{1}{m_0}\left[\boldsymbol{U}^n(t)\right]^T\boldsymbol{U}^n(t)$ at each instant of time (when using weighting matrices other than m_0 in the control cost, see [38]) is given by:

$$\boldsymbol{U}^n(t) = \mathbf{A}^T\left(\mathbf{A}\mathbf{M}_0^{-1}\mathbf{A}^T\right)^+(\boldsymbol{b} - \mathbf{A}\boldsymbol{a}) = m_0\mathbf{A}^+(\boldsymbol{b} - \mathbf{A}\boldsymbol{a}), \tag{10}$$

where the matrix $\mathbf{A}$ and the vector $\boldsymbol{b}$ are given in Eq. (9), $\mathbf{M}_0 = m_0\mathbf{I}$, the vector $\boldsymbol{a}$ is given in Eq. (5), and the superscript '+' denotes the Moore-Penrose generalized inverse of a matrix. In the current case, the matrix $\mathbf{A}$ is the identity matrix such that Eq. (10) simplifies to

$$\boldsymbol{U}^n(t) = m_0(\boldsymbol{b}-\boldsymbol{a}). \tag{11}$$

Hence Eq. (11), which gives the nominal control so that the desired tajectory requiremnet (Eq. 3) is achieved for the nominal system (Eq. 4), is then explicitly obtained as:

$$\boldsymbol{U}^n(t) = m_0\begin{bmatrix} -\frac{n^2\rho}{2}\sin(nt) - \alpha\left[\dot{x} - \frac{n\rho}{2}\cos(nt)\right] - \beta\left[x - \frac{\rho}{2}\sin(nt)\right] - 2\dot{\theta}\dot{y} - \ddot{\theta}x - \dot{\theta}^2 y + \frac{\mu_\oplus}{r_F^3}(x + r_L) - \frac{\mu_\oplus}{r_L^2} \\ -n^2\rho\cos(nt) - \alpha\left[\dot{y} + n\rho\sin(nt)\right] - \beta[y - \rho\cos(nt)] + 2\dot{\theta}\dot{x} + \ddot{\theta}x - \dot{\theta}^2 y + \frac{\mu_\oplus}{r_F^3}y \\ -n^2\rho\sin(nt) - \alpha\left[\dot{z} - n\rho\cos(nt)\right] - \beta[z - \rho\sin(nt)] + \frac{\mu_\oplus}{r_F^3}z \end{bmatrix}, \tag{12}$$

where $r_F = [(x + r_L)^2 + y^2 + z^2]^{1/2}$. It is noted that we have obtained the nominal control force $\boldsymbol{U}^n(t)$ in Eq. (12) in an explicit form that preserves all the nonlinearities of the original dynamical system Eq. (1). However, since Eq. (12) does not consider the uncertain mass m and the disturbance vector $\boldsymbol{D}(t)$, we have to add an additional control input to compensate for their effects, which is the second step of our two-step control procedure, and is developed in the next section.

Design of Robust Adaptive Control for the Nonlinear Uncertain System

When the nominal control force vector $\boldsymbol{U}^n(t)$ that is explicitly obtained in Eq. (12) is added to the nominal system so that

$$m_0\ddot{\boldsymbol{q}}_n = m_0\boldsymbol{a} + \boldsymbol{U}^n, \tag{13}$$

the solution of the displacement vector $\boldsymbol{q}_n(t)$ exactly follows the constraint in Eq. (9) and therefore follows the desired formation trajectory $\boldsymbol{q}_d(t)$. However, the nominal system assumes that $m = m_0$ and it ignores the presence of the uncertainty $\boldsymbol{D}(t)$. In the presence of these uncertainties the vector $\boldsymbol{U}^n(t)$ (Eq. (12)) when used in Eq. (1) will no longer make $\boldsymbol{q}(t) = \boldsymbol{q}_d(t)$; in fact, the solution $\boldsymbol{q}(t)$ obtained from Eq. (1) will deviate, in general, from $\boldsymbol{q}_d(t)$. Thus, to successfully track the desired trajectory $\boldsymbol{q}_d(t)$ in the presence of $m(t, \boldsymbol{q})$ and $\boldsymbol{D}(t)$, we add an additional control force vector $\boldsymbol{U}^c(t)$ that compensates for this deviation so that the general equation of motion of the uncertain system becomes

$$m\ddot{\boldsymbol{q}} = m\boldsymbol{a} + \boldsymbol{D} + \boldsymbol{U}^n + \boldsymbol{U}^c, \tag{14}$$

and the solution $\boldsymbol{q}(t)$ will now successfully track $\boldsymbol{q}_d(t)$. Dividing both sides of Eq. (14) by m, the acceleration of the controlled system is written as

$$\ddot{\boldsymbol{q}} = \boldsymbol{a} + \frac{1}{m}\boldsymbol{D} + \frac{1}{m}\boldsymbol{U}^n + \frac{1}{m}m_0\boldsymbol{u}, \tag{15}$$

where $\boldsymbol{U}^c(t) \triangleq m_0\boldsymbol{u}(t)$ and m_0 is the known nominal mass which is assumed to be constant during the maneuver. It may also be thought of as the best estimate of the average mass of the satellite during the maneuver. The additional robust control force vector $\boldsymbol{U}^c(t)$ in Eq. (15) is divided by the mass $m(t)$ that is time varying and unknown. However, as shall be shown shortly, the effects of $m(t)$ can be incorporated together with the other uncertain terms and the additional control input $\boldsymbol{U}^c(t)$ will successfully compensate for all the uncertainty effects.

In short, the aim is to design a robust adaptive control algorithm that drives the follower satellite to track the desired reference trajectory described in Eq. (3) in which the mass $m(t)$ and the external disturbance $\boldsymbol{D}(t)$ are uncertain. To achieve this goal, we employ the fundamental concept of sliding mode control [11]. First, we design a sliding surface and next, a robust adaptive control strategy is proposed that does not necessitate exact knowledge of the uncertain mass and/or the external disturbance so that the control law is automatically updated in real time. As shall be seen shortly, only the magnitude of control forces is used to update the control law.

Compensating Controller with Known Upper Bound on the Uncertainty

We begin our discussion on developing an adaptive compensating controller, $\boldsymbol{U}^c(t) = m_0\boldsymbol{u}(t)$, that compensates for the uncertainties in the satellite's flight environment and in its dynamical model by initially assuming that an upper bound on these uncertainties is known a priori. We show that under this simplifying assumption, a simple compensating Lyapunov-based constant-gain controller can be readily designed. The following Subsection 4.2 deals with the more realistic situation in which the uncertainty bound is not known a priori.

The performance measure is represented by a 3 by 1 error vector $\boldsymbol{e}(t)$ that is defined by

$$\boldsymbol{e}(t) \triangleq \boldsymbol{q}(t) - \boldsymbol{q}_n(t), \tag{16}$$

where $\boldsymbol{q}(t) = [x(t)\ \ y(t)\ \ z(t)]^T$ is the actual, measured state vector and $\boldsymbol{q}_n(t)$ is the nominal trajectory given in Eq. (13). It is important to note that the error in Eq. (16) is defined as the difference between the actual state vector $\boldsymbol{q}(t)$ and the 'nominal' state vector $\boldsymbol{q}_n(t)$ generated by the solution of Eq. (13) that satisfies the constraint equations Eq. (7) or Eq. (9); it should not be confused with the 'desired' state vector $\boldsymbol{q}_d(t)$ in Eq. (3) that satisfies Eq. (6) with no α and β. Because of the initial errors, $\boldsymbol{q}_n(t)$ will be different from $\boldsymbol{q}_d(t)$ at the initial time. If we define another error vector $\boldsymbol{e}_d(t)$ as

$$\boldsymbol{e}_d(t) \triangleq \boldsymbol{q}_n(t) - \boldsymbol{q}_d(t), \tag{17}$$

it will asymptotically decay to zero as time goes by and the decay rate will depend on the values of α and β selected. The difference between the actual, measured state vector $\boldsymbol{q}(t)$ and the desired one $\boldsymbol{q}_d(t)$ is then given by $\boldsymbol{q}(t) - \boldsymbol{q}_d(t) = \boldsymbol{e}(t) + \boldsymbol{e}_d(t)$. The

compensating controller $\boldsymbol{u}(t)$ will be designed such that the error $\boldsymbol{e}(t)$ defined in Eq. (16) always remains in a user-specified small domain or $\boldsymbol{q}(t) \approx \boldsymbol{q}_n(t)$ for all times, and then $\boldsymbol{q}(t)$ will asymptotically converge to $\boldsymbol{q}_d(t)$ with a desired decay rate because $\boldsymbol{e}(t) + \boldsymbol{e}_d(t) \approx \boldsymbol{e}_d(t)$ and $\boldsymbol{e}_d(t) \to \boldsymbol{0}$ as $t \to \infty$.

The novel idea in this paper is to compensate for the presence of the unknown/uncertain deviation of the actual time-dependent environmental disturbances and the unknown/uncertain deviation of the time-dependent satellite model parameters from those nominally assumed in obtaining $\boldsymbol{q}_n(t)$. This compensation is done by applying an additional compensating control force $\boldsymbol{U}^c(t)$ so that the actual trajectory $\boldsymbol{q}(t)$ in the presence of these unknown/uncertain time-varying disturbances and unknown model parameters always lies within a user-specified 'ball' (however small) around the nominal trajectory $\boldsymbol{q}_n(t)$ which itself continually tends asymptotically to the desired trajectory $\boldsymbol{q}_d(t)$. Thus, the compensating control force so-to-say compensates for the unknown/uncertain environmental and model deviations as though these deviations do not exist at all. Furthermore, this compensating control force $\boldsymbol{U}^c(t)$ is obtained herein adaptively and the bound on these uncertainties is not required to be known.

To achieve this objective, we consider a sliding surface for the SFF system described by Eq. (1):

$$\boldsymbol{s}(t) \triangleq \dot{\boldsymbol{e}}(t) + C\boldsymbol{e}(t), \tag{18}$$

where $\boldsymbol{s}(t) \triangleq [\, s_x(t) \;\; s_y(t) \;\; s_z(t)]^T$ and $\boldsymbol{e}(t) \triangleq [\, e_x(t) \;\; e_y(t) \;\; e_z(t)]^T$ is the error vector defined as Eq. (16). In Eq. (18), C is a positive constant to be selected by the user. It is noted that $\boldsymbol{s}(0) = \boldsymbol{0}$ holds because one can always set $\boldsymbol{q}(0) = \boldsymbol{q}_n(0)$ and $\dot{\boldsymbol{q}}(0) = \dot{\boldsymbol{q}}_n(0)$ where the nominal trajectory $\boldsymbol{q}_n(t)$ is assumed to have nonzero initial errors in the satisfaction of the desired trajectory tracking, and so the sliding mode always starts from the beginning, the system's trajectory starts on the sliding manifold, and there is no "reaching phase" in the sliding dynamics Eq. (18). Also, one can easily show that while the sliding mode $s_i(t) = 0$, $(i = x, y, z)$ holds, the error $e_i(t)$ in each axis asymptotically approaches zero.

In order to ease the controller design process, let us rewrite Eq. (15) as

$$\ddot{\boldsymbol{q}}(t) = \boldsymbol{f}\left(t, \boldsymbol{q}, \dot{\boldsymbol{q}}\right) + \frac{1}{m} m_0 \boldsymbol{u}(t), \tag{19}$$

where $\boldsymbol{f}\left(t, \boldsymbol{q}, \dot{\boldsymbol{q}}\right) \triangleq \boldsymbol{a}\left(t, \boldsymbol{q}, \dot{\boldsymbol{q}}\right) + \frac{1}{m}\boldsymbol{D}(t) + \frac{1}{m}\boldsymbol{U}^n(t)$ is an uncertain term. Then, we have from Eq. (16)

$$\ddot{\boldsymbol{e}}(t) = \ddot{\boldsymbol{q}}(t) - \ddot{\boldsymbol{q}}_n(t) = \left[\boldsymbol{f}\left(t, \boldsymbol{q}, \dot{\boldsymbol{q}}\right) - \ddot{\boldsymbol{q}}_n(t)\right] + \frac{1}{m} m_0 \boldsymbol{u}(t). \tag{20}$$

Also, the time derivative of $\boldsymbol{s}(t)$ in Eq. (18) yields

$$\dot{\boldsymbol{s}}(t) = \ddot{\boldsymbol{e}}(t) + C\dot{\boldsymbol{e}}(t) = \boldsymbol{f}\left(t, \boldsymbol{q}, \dot{\boldsymbol{q}}\right) - \ddot{\boldsymbol{q}}_n(t) + \frac{1}{m} m_0 \boldsymbol{u}(t) + C\dot{\boldsymbol{e}}(t), \tag{21}$$

or more succinctly,

$$\dot{\boldsymbol{s}}(t) = \boldsymbol{g}\left(t, \boldsymbol{q}, \dot{\boldsymbol{q}}\right) + \frac{1}{m} m_0 \boldsymbol{u}(t), \tag{22}$$

where $\boldsymbol{g}\left(t, \boldsymbol{q}, \dot{\boldsymbol{q}}\right) \triangleq \boldsymbol{f}\left(t, \boldsymbol{q}, \dot{\boldsymbol{q}}\right) - \ddot{\boldsymbol{q}}_n(t) + C\dot{\boldsymbol{e}}(t)$ is uncertain.

It is assumed that we cannot accurately know $\boldsymbol{g}$ (t, $\boldsymbol{q}$ $\dot{\boldsymbol{q}}$) and $m(t) > 0$, but they are bounded so that

$$m(t)\|\boldsymbol{g}\left(t, \boldsymbol{q}, \dot{\boldsymbol{q}}\right)\| < \Gamma, \tag{23}$$

where Γ, which is the upper bound on the uncertainties, is an *unknown* positive constant.

Now, we consider the following candidate Lyapunov function:

$$V = \frac{m(t)}{2} \boldsymbol{s}(t)^T \boldsymbol{s}(t). \tag{24}$$

The time derivative of Eq. (24) along the sliding variable trajectory Eq. (22) yields

$$\dot{V} = \frac{\dot{m}}{2} \boldsymbol{s}^T \boldsymbol{s} + m \boldsymbol{s}^T \dot{\boldsymbol{s}} = \frac{\dot{m}}{2} \boldsymbol{s}^T \boldsymbol{s} + m \boldsymbol{s}^T \left(\boldsymbol{g} + \frac{m_0}{m} \boldsymbol{u}\right) = \frac{\dot{m}}{2} \boldsymbol{s}^T \boldsymbol{s} + m \boldsymbol{s}^T \boldsymbol{g} + m_0 \boldsymbol{s}^T \boldsymbol{u}. \tag{25}$$

Recalling Eq. (2) and Eq. (23), we have $\frac{\dot{m}}{2} \boldsymbol{s}^T \boldsymbol{s} \leq 0$ and

$$m|\boldsymbol{s}^T \boldsymbol{g}| \leq \|\boldsymbol{s}\| m \|\boldsymbol{g}\| < \Gamma \|\boldsymbol{s}\|, \tag{26}$$

so that

$$\dot{V} = \frac{\dot{m}}{2} \boldsymbol{s}^T \boldsymbol{s} + m \boldsymbol{s}^T \boldsymbol{g} + m_0 \boldsymbol{s}^T \boldsymbol{u} < \Gamma \|\boldsymbol{s}\| + m_0 \boldsymbol{s}^T \boldsymbol{u}. \tag{27}$$

Given the upper bound Γ that is assumed to be known a priori, the controller $\boldsymbol{U}^c(t)$ that compensates for the system's uncertainties can then be simply designed using

$$\boldsymbol{u} = -\frac{\Gamma}{m_0 \varepsilon} \boldsymbol{s}, \tag{28}$$

where ε is a (small) positive number and then Eq. (27) becomes

$$\dot{V} < \Gamma \|\boldsymbol{s}\| + m_0 \boldsymbol{s}^T \boldsymbol{u} = \Gamma \|\mathrm{s}\| - \frac{\Gamma}{\varepsilon} \|\boldsymbol{s}\|^2 = -\sqrt{\frac{2}{m}} \Gamma \left(\frac{\|\boldsymbol{s}\|}{\varepsilon} - 1\right) \sqrt{\frac{m}{2}} \|\boldsymbol{s}\| = -\mu \cdot V^{1/2}, \tag{29}$$

where $\mu \triangleq \sqrt{\frac{2}{m}} \Gamma \left(\frac{\|\mathrm{s}\|}{\varepsilon} - 1\right)$ is positive parameter in the region where $\|\boldsymbol{s}\| > \varepsilon$ holds. Hence,

the state trajectory of the original dynamics system Eq. (19) controlled by Eq. (28) converges to the region $\|\boldsymbol{s}\| \leq \varepsilon$ in a finite time. We note that the Lyapunov-based compensating controller $\boldsymbol{U}^c(t) \triangleq m_0 \mathrm{u}(t)$ turns out to be simple and has constant gain.

However, as mentioned before, the control law given in Eq. (28) requires a priori knowledge of the bound on the uncertainty, Γ. In real-life situations, an accurate estimation of this bound can be difficult and/or expensive to obtain when controlling a time-varying model of a satellite in an unknown space environment. Estimates of such bounds are often based on experience, intuition, or some other considerations like Earth-based experiments. To encompass such real-life situations in which predictions/estimates of the bounds on the uncertainties encountered during satellite flight-maneuvers may be difficult to obtain or have low/questionable reliability, we next consider an adaptive control law that automatically tunes the gain in real time so that the convergence of the controlled trajectory to the desired one is still guaranteed without any a priori knowledge of the bound Γ on the existing uncertainties.

Adaptive Compensating Controller with Unknown Upper Bound on the Uncertainty

Since the value of the bound Γ on the uncertainty in Eq. (23) is unknown, the control law Eq. (28) is modified to

$$\boldsymbol{u}(t) = -\frac{L(t) + L^*}{m_0 \varepsilon} \boldsymbol{s}(t), \tag{30}$$

where now the unknown constant gain Γ in Eq. (28) has been replaced with a time-varying adaptive gain $L(t) + L^*$, where $L(t) > 0$ for $t \geq 0$, and L^* is a positive constant. The gain $L(t)$ is updated using the adaptation rule

$$\dot{L}(t) = \eta \Big[m_0 \|\boldsymbol{u}(t)\| - L(t) \Big], \quad (L(0) > 0) \tag{31}$$

where η is a user-specified positive constant and m_0 is the nominal value of m used in Eq. (13). In view of Eq. (30), Eq. (31) becomes

$$\dot{L}(t) = \eta \left[L(t) \left(\frac{\|\boldsymbol{s}(t)\|}{\varepsilon} - 1 \right) + \frac{L^*}{\varepsilon} \|\mathrm{s}(t)\| \right]. \quad (L(0) > 0) \tag{32}$$

It is noted that the condition $L(t) \geq L(0) > 0$ is always satisfied. In Eq. (31) $\dot{L}(t)$ has its minimum when $\|\boldsymbol{u}(t)\| = 0$, that is, when $\|\boldsymbol{s}(t)\| = 0$. Eq. (31) then becomes

$$\dot{L}(t) \geq -\eta L(t). \tag{33}$$

The Gronwall's inequality [39] yields

$$L(t) \geq L(0) e^{-\eta t} \geq L(0) > 0. \tag{34}$$

When $\|\boldsymbol{s}(t)\| > \varepsilon$, then from Eq. (32), $\dot{L}(t) > 0$. Hence, for a positive value of the initial condition $L(t_0)$, we have $L(t) \geq L(t_0) > 0$. Here, t_0 is the time instant at which the condition $\|\boldsymbol{s}(t)\| > \varepsilon$ is first satisfied, and $t \geq t_0 \geq 0$. We first prove the following result.

Theorem 1:

Assume that the magnitude of the control force $\boldsymbol{U}^c(t)$ is bounded by the scalar U^* so that

$$m_0\|\boldsymbol{u}(t)\| \leq U^*. \tag{35}$$

When $\|\boldsymbol{s}(t)\| > \varepsilon$, the gain $L(t)$ updated using Eq. (32) has the upper bound U^* for $t \geq t_0 \geq 0$. The initial condition $L(t_0)$ for the gain adaptation rule given in Eq. (32), where t_0 is the time instant at which the condition $\|\boldsymbol{s}(t)\| > \varepsilon$ is first satisfied, can be taken to be any positive number less than U^*. Hence,

$$0 < L(t_0) \leq L(t) < U^*. \tag{36}$$

Proof: From Eq. (30) we have

$$m_0\boldsymbol{u}(t) = -\frac{L(t) + L^*}{\varepsilon}\boldsymbol{s}(t), \tag{37}$$

from which it follows that

$$m_0\|\boldsymbol{u}(t)\| = \frac{L(t) + L^*}{\varepsilon}\|\boldsymbol{s}(t)\|. \tag{38}$$

Assume that $L(t) \geq U^*$ when $\|\boldsymbol{s}(t)\| > \varepsilon$. Then, we find that from Eq. (38)

$$m_0\|\boldsymbol{u}(t)\| = \frac{\|\boldsymbol{s}(t)\|}{\varepsilon}\left[L(t) + L^*\right] > U^* + L^* > U^*, \tag{39}$$

which contradicts the relation $m_0\|\boldsymbol{u}(t)\| \leq U^*$ that is given in Eq. (35). Hence, our assumption that $L(t) \geq U^*$ is incorrect, and therefore $L(t) < U^*$. Thus, when $\|\boldsymbol{s}(t)\| > \varepsilon$ and $t \geq t_0 \geq 0$,

$$0 < L(t_0) \leq L(t) < U^*, \tag{40}$$

which completes the proof.

We are now ready to state the adaptive control approach to be used for $t \geq t_0 \geq 0$ as long as $\|\boldsymbol{s}(t)\| > \varepsilon$ where t_0 is the time instant at which the condition $\|\boldsymbol{s}(t)\| > \varepsilon$ is first satisfied.

Theorem 2:

Assume that the control force has an upper limit U^* such that $m_0\|\boldsymbol{u}(t)\| \le U^*$ and $U^* \ge \Gamma$. Then the control law given in Eq. (30), along with the gain adaptation law given in Eq. (31) or (32) and any initial condition $0 < L(t_0) < U^*$ will cause the sliding variable $\boldsymbol{s}(t)$ given in Eq. (18) to converge to the region $\|\boldsymbol{s}(t)\| \le \varepsilon$. Here, t_0 is the time instant at which the condition $\|\boldsymbol{s}(t)\| > \varepsilon$ is first satisfied. The constants η and L^* are user-defined positive constants. Also, the error is confined in the region $\|\boldsymbol{e}(t)\| \le \frac{\varepsilon}{C}$.

Proof: Let us define the following Lyapunov function (to reduce clutter, we often do not show L as an explicit function of time t)

$$V(t) = \frac{m(t)}{2}\boldsymbol{s}(t)^T\boldsymbol{s}(t) + \frac{1}{2\gamma}\left(L(t) - U^*\right)^2, t \ge t_0 \ge 0 \tag{41}$$

where $L(t) < U^*$ by Theorem 1, and γ is a positive constant that will be chosen shortly. Then, for $\|\boldsymbol{s}(t)\| > \varepsilon$ the time derivative of Eq. (41) on successively using Eqs. (22), (37), (26), the Cauchy-Schwarz inequality, and Eq. (23) yields

$$\begin{aligned}
\dot{V} &= \frac{\dot{m}}{2}\boldsymbol{s}^T\boldsymbol{s} + m\boldsymbol{s}^T\dot{\boldsymbol{s}} + \frac{1}{\gamma}\left(L - U^*\right)\dot{L} \\
&= \frac{\dot{m}}{2}\boldsymbol{s}^T\boldsymbol{s} + m\boldsymbol{s}^T\left(\boldsymbol{g} + \frac{m_0}{m}\boldsymbol{u}\right) + \frac{1}{\gamma}\left(L - U^*\right)\dot{L} \\
&= \frac{\dot{m}}{2}\boldsymbol{s}^T\boldsymbol{s} + m\boldsymbol{s}^T\boldsymbol{g} - \frac{L}{\varepsilon}\boldsymbol{s}^T\boldsymbol{s} - \frac{1}{\gamma}\left(U^* - L\right)\dot{L} - \frac{L^*}{\varepsilon}\boldsymbol{s}^T\boldsymbol{s} \\
&< \Gamma\|\boldsymbol{s}\| - \frac{L}{\varepsilon}\|\boldsymbol{s}\|^2 - \frac{1}{\gamma}\left(U^* - L\right)\dot{L} - \frac{L^*}{\varepsilon}\|\boldsymbol{s}\|^2.
\end{aligned} \tag{42}$$

The last inequality follows from the fact $\frac{\dot{m}}{2}\boldsymbol{s}^T\boldsymbol{s} \le 0$ and Eq. (26). Noting further that $\frac{\|\boldsymbol{s}\|^2}{\varepsilon} > \|\boldsymbol{s}\|$, we obtain

$$\begin{aligned}
\dot{V} &< \Gamma\|\boldsymbol{s}\| - L\|\boldsymbol{s}\| - \frac{1}{\gamma}\left(U^* - L\right)\dot{L} - L^*\|\boldsymbol{s}\| = \|\boldsymbol{s}\|(\Gamma - L) - \frac{1}{\gamma}\left(U^* - L\right)\dot{L} - L^*\|\boldsymbol{s}\| \\
&= \|\boldsymbol{s}\|(\Gamma - L) - \frac{1}{\gamma}\left(U^* - L\right)\dot{L} + \|\boldsymbol{s}\|\left(U^* - L\right) - \|\boldsymbol{s}\|\left(U^* - L\right) - L^*\|\boldsymbol{s}\| \\
&= \|\boldsymbol{s}\|\left(\Gamma - U^*\right) - L^*\|\boldsymbol{s}\| - \frac{1}{\gamma}\left(U^* - L\right)\dot{L} + \|\boldsymbol{s}\|\left(U^* - L\right) \\
&= -\|\boldsymbol{s}\|\left(U^* - \Gamma + L^*\right) - \left(U^* - L\right)\left(\frac{1}{\gamma}\dot{L} - \|\boldsymbol{s}\|\right).
\end{aligned} \tag{43}$$

In the last equality the first member on the right-hand side is positive because $U^* \geq \Gamma$ is assumed. Also, by Eq. (40), $U^* - L > 0$ is satisfied when $\|\boldsymbol{s}\| > \varepsilon$ in the second member on the right.

Thus, to ensure that $\dot{V} < 0$ we then need to find a γ such that the inequality $\frac{1}{\gamma}\dot{L} - \|\boldsymbol{s}\| \geq 0$ holds when $\|\boldsymbol{s}\| > \varepsilon$ and $t \geq t_0 \geq 0$. This relation requires that we choose a value of γ such that

$$\gamma \leq \frac{\dot{L}}{\|\boldsymbol{s}\|} = \eta \left[L\left(\frac{1}{\varepsilon} - \frac{1}{\|\boldsymbol{s}\|}\right) + \frac{L^*}{\varepsilon} \right], t \geq t_0 \geq 0. \tag{44}$$

We have shown when γ is less than or equal to the quantity on the right-hand side of the inequality in Eq. (44) for $t \geq t_0 \geq 0$ and $\|\boldsymbol{s}\| > \varepsilon$, then $\dot{V}$ is guaranteed to be negative. Since $0 < L(t_0) \leq L(t)$ (see Eq. (40)) for $t \geq t_0 \geq 0$, using Eq. (44) we can choose

$$\gamma \leq \eta \left[L(t_0)\left(\frac{1}{\varepsilon} - \frac{1}{\|\boldsymbol{s}\|}\right) + \frac{L^*}{\varepsilon} \right], t \geq t_0 \geq 0. \tag{45}$$

The first term on the right hand side of Eq. (45) is positive when $\|\boldsymbol{s}\| > \varepsilon$ since the quantity in the round bracket is positive. Hence, it would suffice to choose $\gamma \triangleq \gamma_0 = \frac{\eta L^*}{\varepsilon} > 0$, so that the inequality in Eq. (45) is met for $t \geq t_0 \geq 0$. Thus, with $\gamma = \gamma_0$ in Eq. (41), $\dot{V} < 0$ when $\|\boldsymbol{s}\| > \varepsilon$. Finally, it can be shown that while the condition $\|\boldsymbol{s}\| \leq \varepsilon$ is satisfied, from Eq. (18) the error is confined within the region $\|\boldsymbol{e}(t)\| \leq \frac{\varepsilon}{C}$ [25].

Simulation Results

The new two-step adaptive control approach proposed in Section 4 is applied to precision control of satellite formation flight (SFF) in the face of model and environmental uncertainties. The aim is to validate the approach and assess its effectiveness through simulations. A desired relative configuration that has a projected circular formation in the y-z plane with a 1 km formation radius ($\rho = 1$ km) is considered (Eq. (3)).

The SFF system parameters and the orbital parameters of the leader satellite used for the numerical simulation are listed in Table 1, where r_p is the distance between the Earth center and the leader satellite at the perigee, and the orbital elements $\boldsymbol{e}$, i, $\boldsymbol{\Omega}$, ω,

Table 1 Orbital and system parameters

Parameters	Values
m_0, kg	10
$\mu_\oplus$, km$^3 \cdot$ s^{-2}	398,600
r_p. km	6878
e	0.2
i, deg	97.4
Ω, deg	0
ω, deg	0
M_0, deg	0

and M_0 are the eccentricity, the inclination, the right ascension of the ascending node, the argument of perigee, and the mean anomaly at the initial position of the leader satellite, respectively. All the simulations are carried out in the MATLAB/Simulink environment. A fixed time-step ode4 Runge-Kutta integrator is used throughout to more closely reflect the capabilities of embedded on-board micro-controllers usually employed in real-life satellite maneuvers; the time step is taken to be 0.1 s.

The disturbance force $\boldsymbol{D}(t)$ acting on the follower satellite is given by (in N)

$$\begin{bmatrix} D_x \\ D_y \\ D_z \end{bmatrix} = 1.2 \times 10^{-3} \begin{bmatrix} 1-1.5\sin(nt) \\ 0.5\sin(2nt) \\ \sin(nt) \end{bmatrix}, \tag{46}$$

where n is the mean angular velocity which is equal to $\sqrt{\mu_\oplus / a_L^3}$ (a_L is the semimajor axis of the leader satellite). The disturbance force, Eq. (46), incorporates gravitational perturbations, atmospheric drag, and solar radiation pressure forces, and its magnitude is greater by at least an order of magnitude than what has been used previously [5, 6, 18].

While it is commonly known how to compute $\theta(t)$ in Eq. (5), for the sake of completeness, we briefly outline this here. Since the argument of perigee (ω) is zero in our application from Table 1, the true argument of latitude $\theta(t)$ is equal to the true anomaly. First, from time t we obtain the mean anomaly $M(t)$ such that $M(t) = nt$, where n is the mean motion. Next, the eccentric anomaly $E(t)$ is obtained by solving the Kepler's equation [31]

$$M(t) = E(t) - e\sin(E(t)), \tag{47}$$

where e is the eccentricity. Finally, the true anomaly $\theta(t)$ is calculated as [31]

$$\theta(t) = 2\tan^{-1}\left(\sqrt{\frac{1+e}{1-e}}\tan\left(\frac{E(t)}{2}\right)\right). \tag{48}$$

The initial states for the numerical simulation are as follows:

$$\boldsymbol{q}(0) = [\,100 \quad 1100 \quad 100\,]^T \text{ (m)}, \quad \dot{\boldsymbol{q}}(0) = [\,0.396 \quad 0 \quad 0.792\,]^T \text{ (m/s)}. \tag{49}$$

First, let us consider the case where there is no disturbance $\boldsymbol{D}(t)$ and the mass of the follower satellite has a known constant value of $m_0 = 10$ kg. The control force $\mathrm{U}^n(t)$ explicitly given in Eq. (12) is applied to this nominal system, where $\alpha = 5.1 \times 10^{-3}$, $\beta = 6.5 \times 10^{-6}$ are selected such that the system Eq. (7) is critically damped since $\alpha^2 - 4\beta = 0$. Fig. 1 shows the controlled trajectory in 3-dimensional space (upper left), projected onto y-z plane (upper right), projected onto x-z plane (bottom left), and projected onto x-y plane (bottom right). We have, as noted before, ignored any change in the mass of the satellite from its nominal value during the actual maneuver and also the presence of any environmental disturbances during the maneuver. It is clearly seen that the controlled trajectory successfully merges into the desired projected circular orbit in

the y-z plane, the projected straight line in the x-z plane, and the projected elliptical orbit in the x-y plane. It should be noted that this nominal trajectory tends exactly to the desired trajectory at the user-specified rate given in Eq. (7). Figure 2 depicts relative position errors $\boldsymbol{q}(t)-\boldsymbol{q}_d(t)$ in the satisfaction of the desired trajectory (Eq. (3)) along each axis and the control thrust demand. Note that the relative errors $\boldsymbol{q}(t)-\boldsymbol{q}_d(t)$ are equal to $\boldsymbol{e}(t)+\boldsymbol{e}_d(t)$ defined in Eqs. (16) and (17), respectively, and since $\boldsymbol{U}^n(t)$ is the exact control force, $\boldsymbol{e}(t)=\boldsymbol{q}(t)-\boldsymbol{q}_n(t)=\boldsymbol{0}$ is maintained throughout the maneuver and since $\boldsymbol{q}_n(t)$ asymptotically approaches $\boldsymbol{q}_d(t)$ at a rate described by Eq. (7), $\boldsymbol{q}(t)$ also converges to $\boldsymbol{q}_d(t)$ at the same rate. The x-axis denotes time normalized by the orbital period of the leader satellite. It is observed that despite the 100 m initial position offset on all three axes the controlled trajectory of the follower satellite tends to $\boldsymbol{q}_d(t)$. The error $\boldsymbol{q}(t)-\boldsymbol{q}_n(t)$, which is critically damped, asymptotically decays to zero as described by Eq. (7). The steady-state error is seen to be extremely small and is of the order of 10^{-12} m.

Now, we consider the case where the disturbance $\boldsymbol{D}(t)$ given by Eq. (46) is imposed on the system and the mass of the follower is uncertain, time-varying, and governed by Eq. (2), $\dot{m}(t)=-\lambda\|\boldsymbol{U}(t)\|$, where $\lambda=8.0\times10^{-5}$ s/m and the initial mass is $m(0)=$ 10 kg. If we apply only the nominal control force calculated by Eq. (12) to this uncertain system along with the environmental disturbance $\boldsymbol{D}(t)$, we expect that the error in the satisfaction of the desired trajectory Eq. (3) does not necessarily converge to zero, because of the inclusion of the addition of the uncertain terms in Eq. (15).

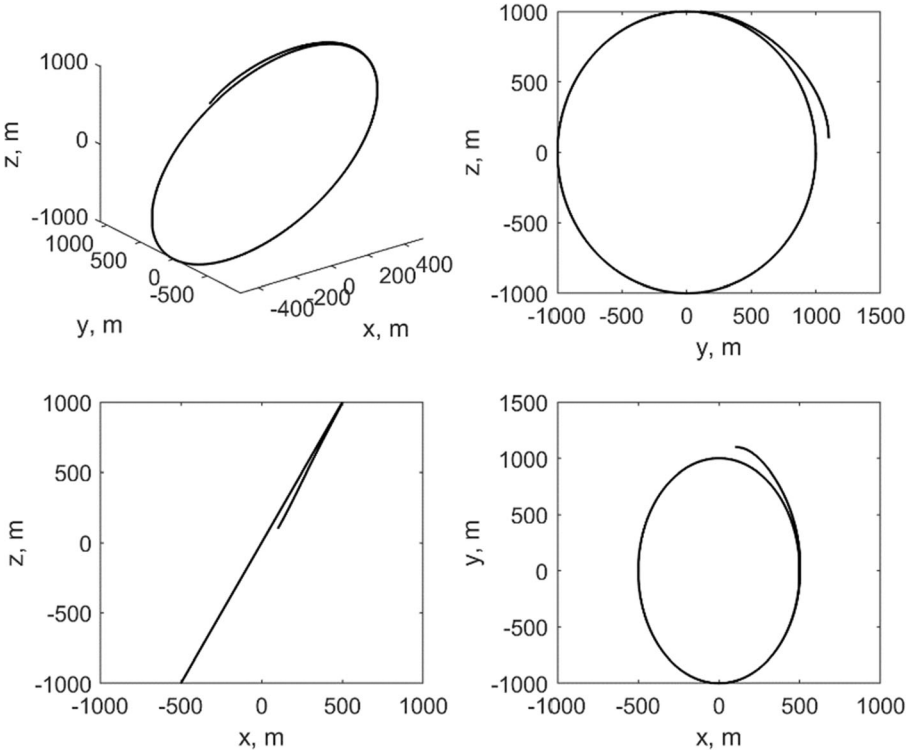

Fig. 1 Controlled trajectory of the follower satellite obtained by control force $\boldsymbol{U}^n(t)$ for nominal system

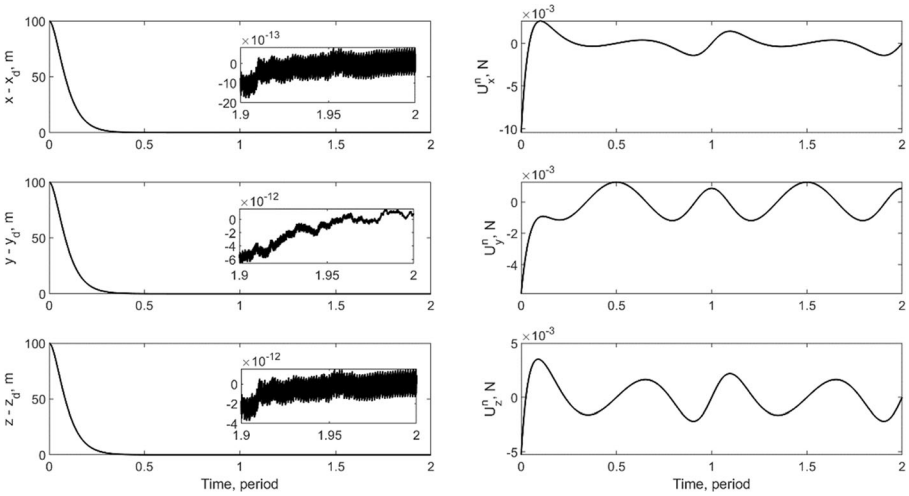

Fig. 2 Relative position errors and thrust demand obtained by control force $\boldsymbol{U}^n(t)$ for nominal system

Figure 3 shows the relative position errors $\boldsymbol{q}(t) - \boldsymbol{q}_d(t) = \boldsymbol{e}(t) + \boldsymbol{e}_d(t)$ and the control thrust in each axis. As expected, the controlled trajectory does not merge onto the desired projected circular trajectory and there exists a large error along each axis. More specifically, due to the uncertainties caused by the mass and the external disturbance, the actual position vector $\boldsymbol{q}(t)$ fails to track the nominal trajectory $\boldsymbol{q}_n(t)$ although $\boldsymbol{q}_n(t)$ still converges to $\boldsymbol{q}_d(t)$ as time goes by.

Now let us add the smooth adaptive compensating control force $\boldsymbol{U}^c(t)$ calculated by Eq. (30) with the gain adaptation law given in Eq. (31). The sliding surface is selected as in Eq. (18) with $C = 1$ and the selected control parameters are

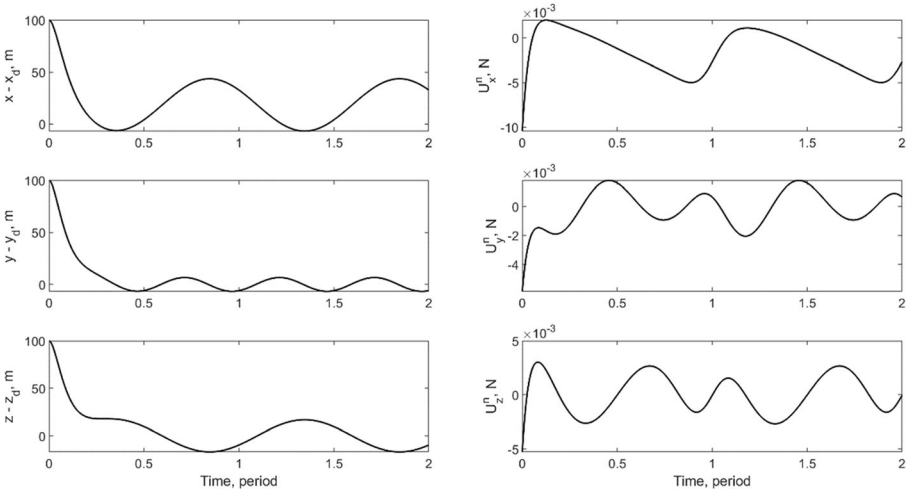

Fig. 3 Relative position errors and thrust demand obtained by control force $\boldsymbol{U}^n(t)$ in the presence of disturbance and uncertain mass

$$\varepsilon = 0.01, \eta = 0.1, L^* = 1, L(0) = 0.002. \tag{50}$$

The novel idea herein is focused on compensation for the effects of the unknown/uncertain actual time-dependent environmental disturbances and satellite model parameters—in our case, the external disturbance force and the actual unknown, time-varying mass of the follower satellite during the maneuver. An additional compensating force $\boldsymbol{U}^c(t)$ is applied so that despite these disturbances and uncertainties the actual trajectory $\boldsymbol{q}(t)$ always lies within a user-defined small 'ball' around the nominal trajectory $\boldsymbol{q}_n(t)$ which itself, as stated before, asymptotically approaches the desired trajectory $\boldsymbol{q}_d(t)$. In addition, this compensating control force $\boldsymbol{U}^c(t)$ is obtained in an adaptive manner without needing the information about the bound on these uncertainties.

Starting with the same initial conditions given in Eq. (49), Fig. 4 shows the time history of the relative position errors $\boldsymbol{q}(t) - \boldsymbol{q}_d(t) = \boldsymbol{e}(t) + \boldsymbol{e}_d(t)$, and the control thrust is provided when the sum of the two control forces $\boldsymbol{U}^n(t)$ obtained by Eq. (12) and $\boldsymbol{U}^c(t)$ is applied to the uncertain system. The application of the additive control force $\boldsymbol{U}^c(t)$ greatly improves the control accuracy and the steady-state error is extremely small and of order 10^{-5} m in the x-direction and 10^{-6} m in the y- and z-directions. The controlled trajectory is the same as the one shown in Fig. 2 because the additive control $\boldsymbol{U}^c(t)$ has been designed to track the reference trajectory given in Eq. (3). More specifically, the error $\boldsymbol{e}(t) = \boldsymbol{q}(t) - \boldsymbol{q}_n(t)$ is extremely small (see Fig. 8) such that both $\boldsymbol{q}(t)$ and $\boldsymbol{q}_n(t)$ successfully converge to the desired trajectory $\boldsymbol{q}_d(t)$ with a desired rate. This can also be seen in Fig. 5 where the additive control force $\boldsymbol{U}^c(t)$ is depicted in comparison with the disturbance force $\boldsymbol{D}(t)$ for each axis. The disturbance is to a good extent eliminated by the application of the additive control force obtained by using the smooth adaptive sliding mode control developed in Subsection 4.2. This is because the unknown variation in the mass of the satellite over the period of integration, which the

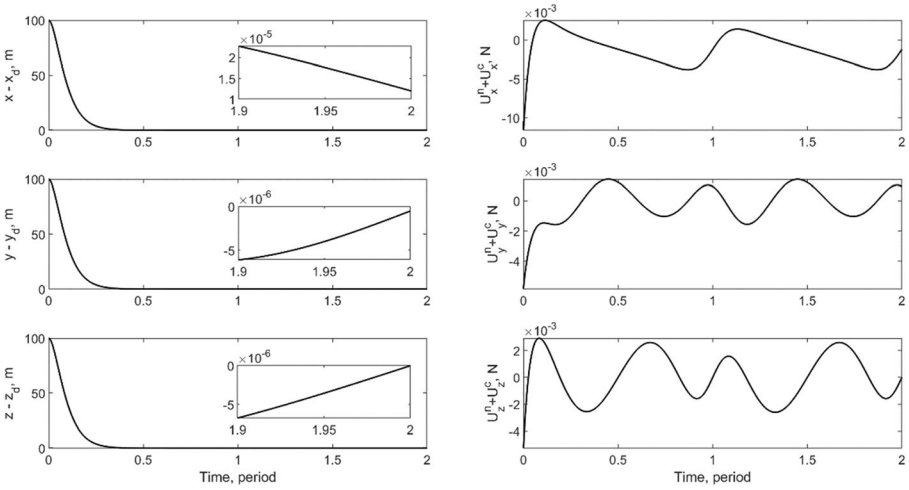

Fig. 4 Relative position errors and thrust demand obtained by applying both $\boldsymbol{U}^n(t)$ and $\boldsymbol{U}^c(t)$ in the presence of unknown/uncertain disturbance and unknown/uncertain follower satellite mass with $\alpha = 5.1 \times 10^{-3}$, $\beta = 6.5 \times 10^{-6}$

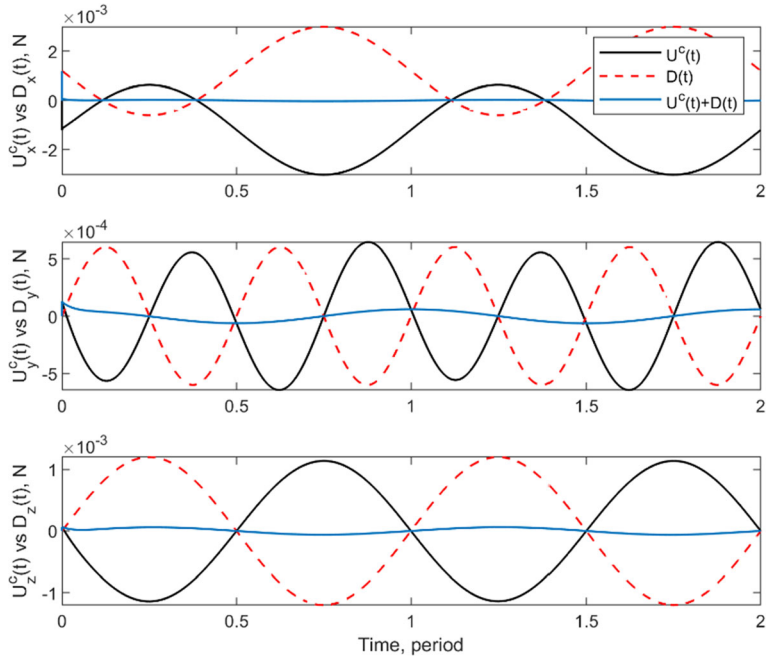

Fig. 5 Adaptive control force $\boldsymbol{U}^c(t)$, disturbance $\boldsymbol{D}(t)$, and $\boldsymbol{U}^c(t) + \boldsymbol{D}(t)$

adaptive control $\boldsymbol{U}^c(t)$ also compensates for, is not appreciable, as shown later (see Fig. 10). With the disturbance nearly eliminated, the control $\boldsymbol{U}^n(t)$ then successfully

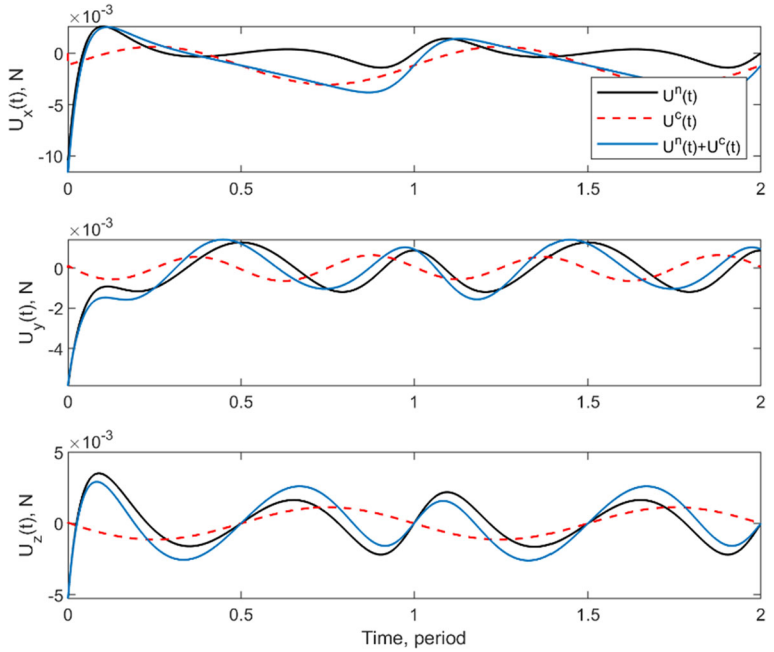

Fig. 6 Comparison of nominal control force $\boldsymbol{U}^n(t)$, adaptive control force $\boldsymbol{U}^c(t)$, and $\boldsymbol{U}^n(t) + \boldsymbol{U}^c(t)$

tracks the desired trajectory. More specifically, from Eqs. (13) and (14), the error between the actual trajectory and the nominal trajectory is calculated as

$$\ddot{\boldsymbol{e}}(t) = \ddot{\boldsymbol{q}}(t) - \ddot{\boldsymbol{q}}_n(t) = \frac{1}{m(t)}\left[\boldsymbol{D}(t) + \left(1 - \frac{m(t)}{m_0}\right)\boldsymbol{U}^n(t) + \boldsymbol{U}^c(t)\right]. \tag{51}$$

As mentioned before, the mass $m(t)$ of the follower satellite does not deviate much from the nominal mass m_0 throughout the maneuver and the magnitude of $\ddot{\boldsymbol{e}}(t)$ remains pretty small, the magnitude of the sum of $\boldsymbol{U}^c(t) + \boldsymbol{D}(t)$ also should be small, which explains Fig. 5. The three control thrust functions $\boldsymbol{U}^n(t)$, $\boldsymbol{U}^c(t)$, and $\boldsymbol{U}^n(t) + \boldsymbol{U}^c(t)$ for each axis are compared with one another in Fig. 6. We can see that the amplitude of the adaptive sliding mode control force $\boldsymbol{U}^c(t)$ is of the same order of magnitude as the nominal control force $\boldsymbol{U}^n(t)$. The nominal control command $\boldsymbol{U}^n(t)$ enables exact tracking of the nominal trajectory while the robust control command $\boldsymbol{U}^c(t)$ mitigates the effects of uncertain environmental disturbances and uncertain mass variations such that the disturbed, uncertain system behaves as the nominal system.

Figure 7 depicts the time history of the sliding variable $\boldsymbol{s}(t)$ for each axis (upper part) and the ratio $\frac{\|\boldsymbol{s}(t)\|}{\varepsilon}$ (lower part). It can be seen that the sliding variable is well confined within the region $\|\boldsymbol{s}(t)\| \le \varepsilon = 0.01$. Also, by defining the error as in Eq. (16), the sliding variable $\boldsymbol{s}(t)$ starts from zero. This shows the difference between the current approach and the approach commonly adopted in the sliding mode control literature in which

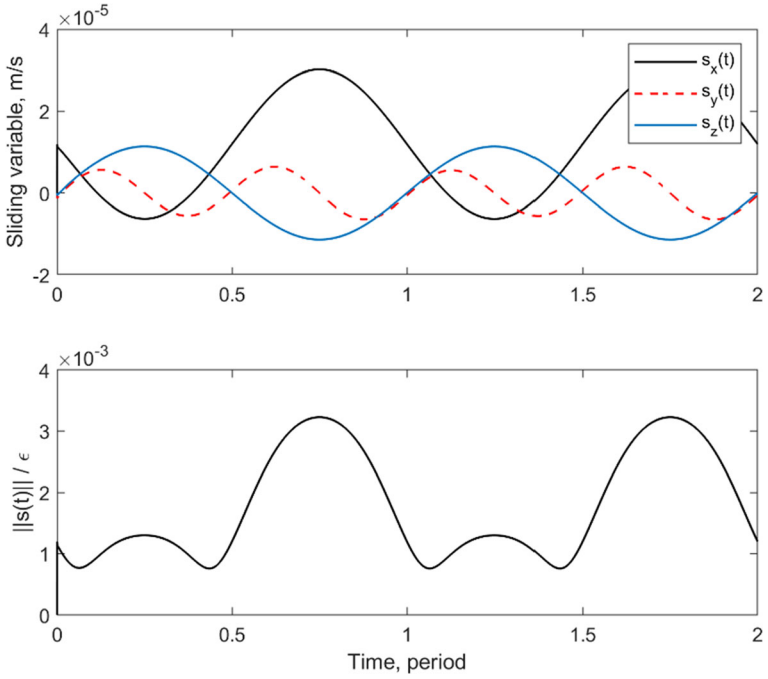

Fig. 7 Time history of sliding variable $\boldsymbol{s}(t)$ and the ratio $\frac{\|\boldsymbol{s}(t)\|}{\varepsilon}$

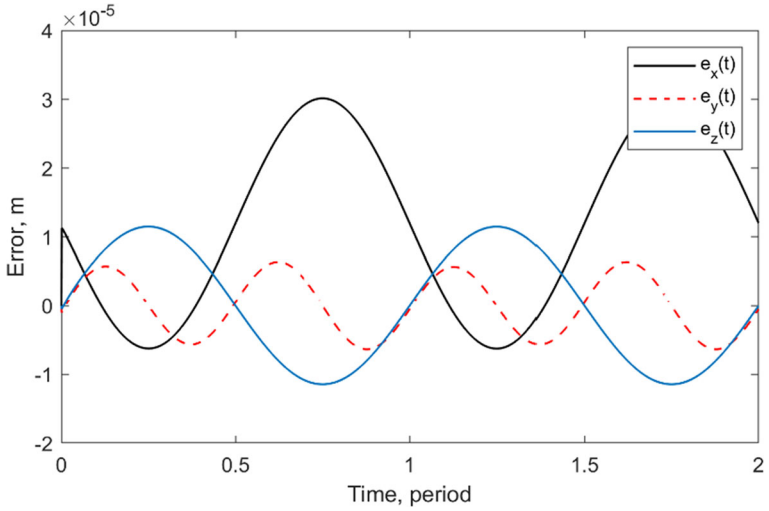

Fig. 8 Time history of error $\boldsymbol{e}(t)$

considerable difficulty is encountered in trying to remove the so-called 'reaching phase' [40, 41]. Figure 8 represents the time history of the error defined as in Eq. (16) for each axis. As shown in Theorem 2, the error is well confined within the region $\|\boldsymbol{e}(t)\| \leq \frac{\varepsilon}{C} = 0.01$.

Figure 9 shows the time history of the gain $L(t)$ obtained as in Eq. (31). The initial gain is selected as $L(0) = 0.002$ and it is seen that the gain is always positive throughout the maneuver. Figure 10 shows the variation of the mass $m(t)$. The mass is obtained by integrating Eq. (2) where $\boldsymbol{U}(t) = \boldsymbol{U}^n(t) + \boldsymbol{U}^c(t)$ with the initial condition $m(0) = m_0$. It is found that after the two-period maneuver the final mass is about 9.9963 kg, a change of only 0.0037 kg (i.e., mass loss of 0.037%) due to the high specific impulse of the Hall thruster used.

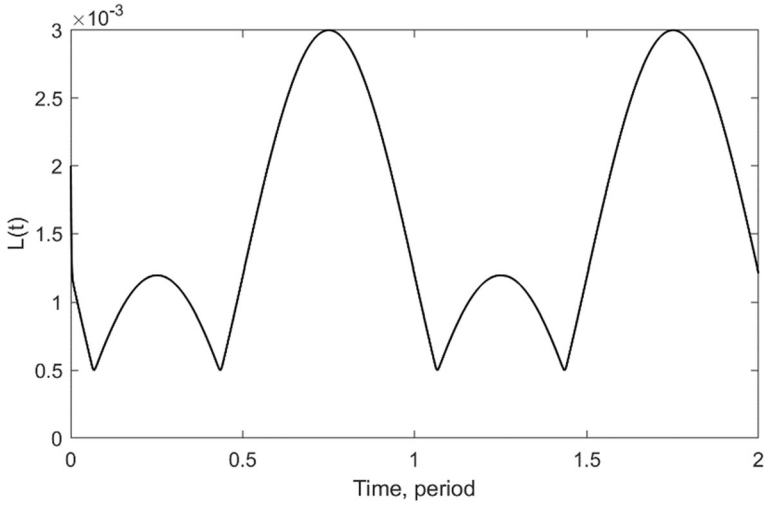

Fig. 9 Time history of gain $L(t)$

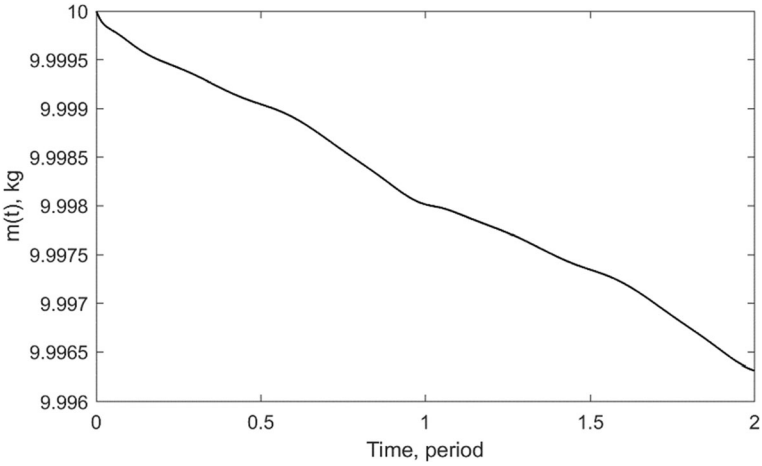

Fig. 10 Time history of mass $m(t)$

Finally, we consider the performance of our control methodology in the presence of limitations placed on the magnitude of the control thrust force. More specifically, it is assumed that the total control input $\boldsymbol{U}(t) = \boldsymbol{U}^n(t) + \boldsymbol{U}^c(t)$ gets saturated at 8 mN in each direction. It is expected from Figs. 4 and 6 that the control forces are saturated early in the transient phase especially in the x-direction because of the initial offset errors. Figure 11 shows the time history of the relative position errors $\boldsymbol{q}(t) - \boldsymbol{q}_d(t) = \boldsymbol{e}(t) + \boldsymbol{e}_d(t)$ and the control thrust demand $\boldsymbol{U}^n(t) + \boldsymbol{U}^c(t)$ is provided. As expected, the control thrust in the x-direction shows bang-bang like control nearly up to about a fifth of the period of the leader satellite because of control thrust saturation. Its y-component is also affected because the x- and y-components are highly coupled with each other as expected from the linearized dynamics of relative motion obtained from the Tschauner-Hempel equations [3]. Nonetheless, as seen in Fig. 11, the steady-state error along each coordinate axis is commensurate with the case with no saturation shown in

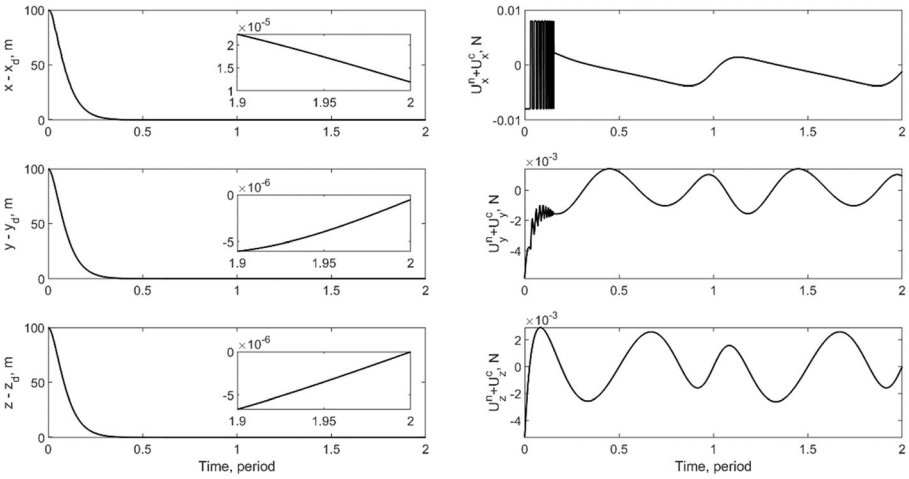

Fig. 11 Relative position errors and thrust demand obtained by applying both $\boldsymbol{U}^n(t)$ and $\boldsymbol{U}^c(t)$ in the presence of disturbance and uncertain mass when control thrust is saturated at 8 mN with $\alpha = 5.1 \times 10^{-3}$, $\beta = 6.5 \times 10^{-6}$

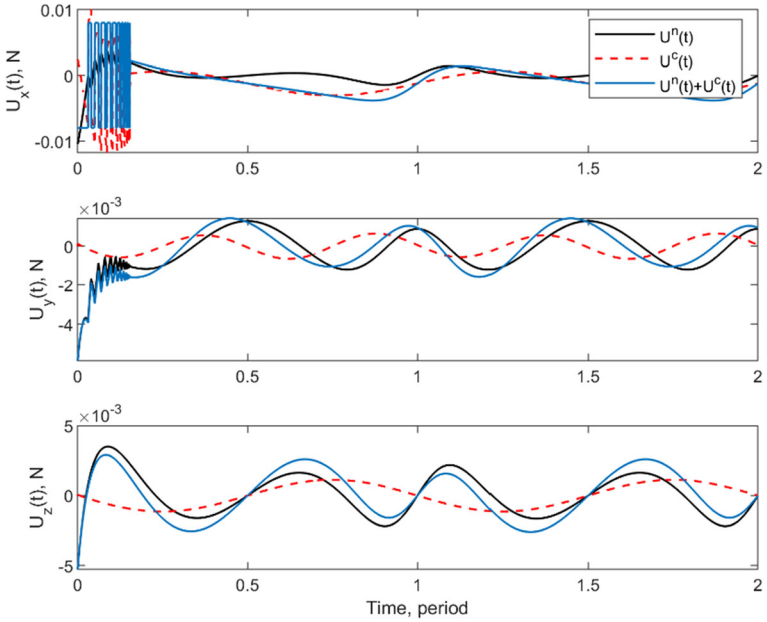

Fig. 12 Comparison of nominal control force $\boldsymbol{U}^n(t)$, adaptive control force $\boldsymbol{U}^c(t)$, and $\boldsymbol{U}^n(t) + \boldsymbol{U}^c(t)$ when control thrust is saturated at 8 mN with $\alpha = 5.1 \times 10^{-3}$, $\beta = 6.5 \times 10^{-6}$

Fig. 4. The three control inputs $\boldsymbol{U}^n(t)$, $\boldsymbol{U}^c(t)$, and $\boldsymbol{U}^n(t) + \boldsymbol{U}^c(t)$ for each axis are shown in Fig. 12. Although each of the two inputs $\boldsymbol{U}^n(t)$ and $\boldsymbol{U}^c(t)$ may exceed the saturation limit (8 mN), their sum always stays within the limit. Figure 13 shows the variation of the mass $m(t)$. It can be seen that the final mass is about 9.9959 kg, a change of 0.0041 kg (i.e., mass loss of 0.041%), which is a slightly greater mass loss than when there is no limitation on the control thrust (see Fig. 10).

One way to avoid control input saturation is by increasing the settling time to reach the desired trajectory, which is achieved by appropriately selecting the values of α or β

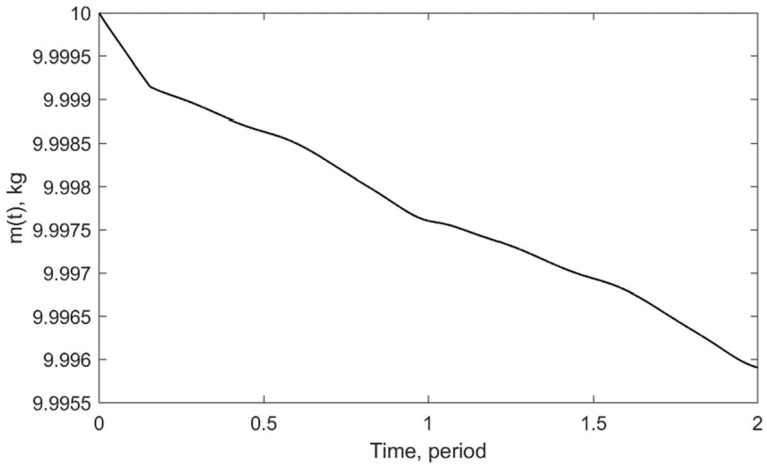

Fig. 13 Time history of mass $m(t)$ when control thrust is saturated at 8 mN with $\alpha = 5.1 \times 10^{-3}$, $\beta = 6.5 \times 10^{-6}$

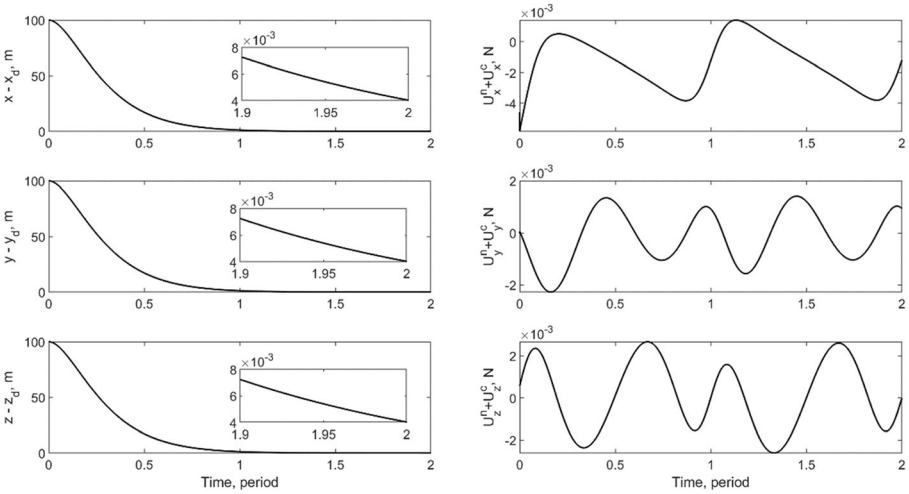

Fig. 14 Relative position errors and thrust demand obtained by applying both $\boldsymbol{U}^n(t)$ and $\boldsymbol{U}^c(t)$ in the presence of disturbance and uncertain mass with $\alpha = 1.6 \times 10^{-3}$, $\beta = 6.5 \times 10^{-7}$

in Eq. (7) [42]. Using this approach, Fig. 14 shows tracking errors over two time periods of the leader satellite, and the required control thrust demand when $\alpha = 1.6 \times 10^{-3}$, $\beta = 6.5 \times 10^{-7}$. By adjusting α and β so that the settling time becomes longer, control thrust demands that do not reach saturation can be thus obtained. Figure 15 shows the corresponding variation of the mass of the follower satellite. The final mass is now about 9.9964 kg, a change of 0.0036 kg (i.e., mass loss of 0.036%), which saves a little more fuel than the control thrust saturation (see Fig. 13). As for the larger errors seen in Fig. 14 when compared with Fig. 4, the smaller values of α or β cause slower convergence of $\boldsymbol{q}_n(t)$ to $\boldsymbol{q}_d(t)$, and so over the time horizon of two orbital periods shown the corresponding tracking errors are larger. This is verified in Fig. 16, where even smaller values of $\alpha = 1.1 \times 10^{-3}$, $\beta = 3.0 \times 10^{-7}$ are used, leading to an even longer settling time; the simulation is now done for six orbital periods of the leader satellite. As

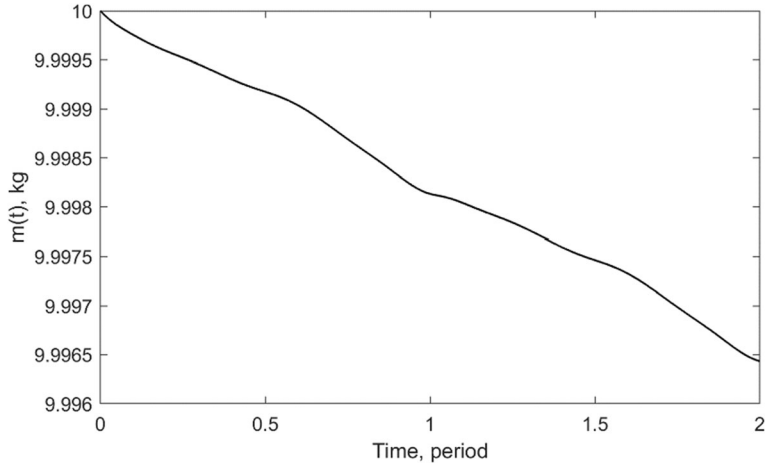

Fig. 15 Time history of mass $m(t)$ with $\alpha = 1.6 \times 10^{-3}$, $\beta = 6.5 \times 10^{-7}$

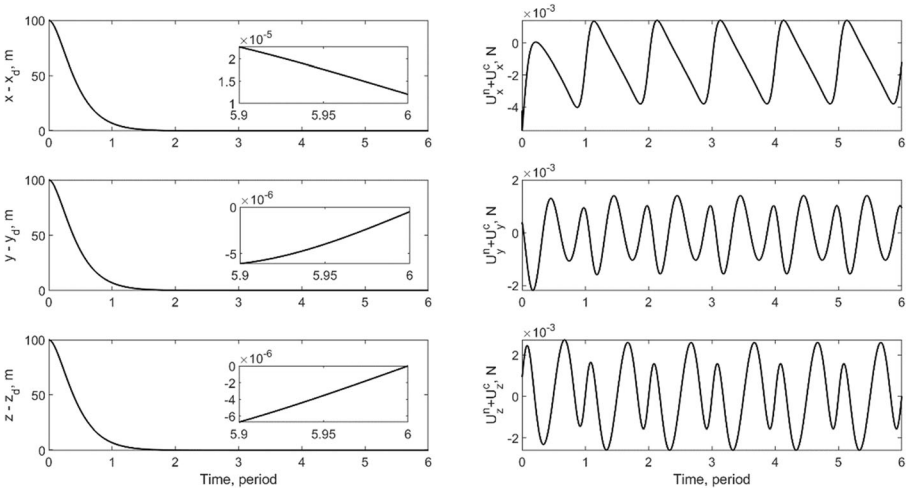

Fig. 16 Relative position errors and thrust demand obtained by applying both $\boldsymbol{U}^n(t)$ and $\boldsymbol{U}^c(t)$ in the presence of disturbance and uncertain mass with $\alpha = 1.1 \times 10^{-3}$, $\beta = 3.0 \times 10^{-7}$

seen in this figure, the final errors, near the end of the simulation time, are of the same order of magnitude as those shown in Fig. 4, and the control thrust shows no saturation. Figure 17 depicts the variation of the mass of the follower satellite. The mass after the two-period maneuver is 9.9964 kg, a change of 0.0036 kg (mass loss of 0.036%) and the final mass (after the six-period maneuver) is 9.9896 kg, a change of 0.0104 kg (mass loss of 0.104%).

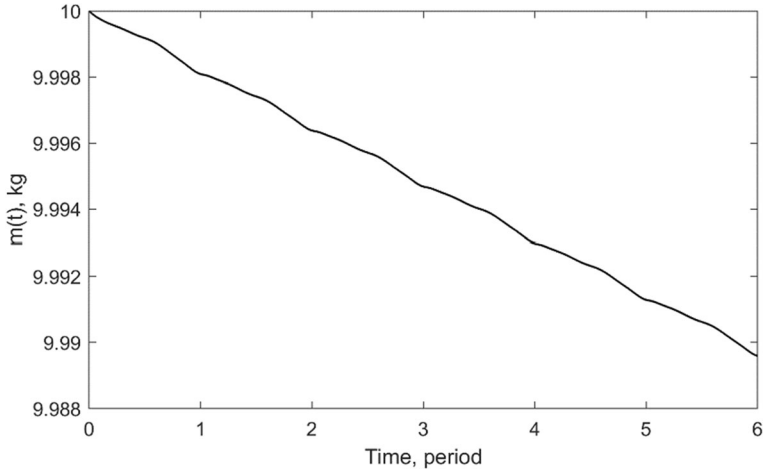

Fig. 17 Time history of mass $m(t)$ with $\alpha = 1.1 \times 10^{-3}$, $\beta = 3.0 \times 10^{-7}$

Conclusion

In this paper a new on-orbit autonomous control methodology is proposed for precision formation flight of satellites in the presence of uncertainties in the description of their physical models and in the description of the environmental fields through which the formation moves. The methodology is used to precisely track the desired relative trajectories between two satellites flying in formation. In the first step of the methodology, a nominal deterministic system is considered in which the uncertain parameters in the satellite model are replaced by their best estimates and the uncertain fields are deterministically described using their best representations. Despite large initial deviations from the desired formation configuration, closed-form control to exactly track the nominal trajectory is obtained. This control minimizes a desired quadratic cost function of the control force at each instant of time and is based on results from analytical dynamics. It provides an explicit solution and there are no linearizations/approximations of the nonlinear system.

The second step of the control methodology deals with handling the presence of uncertainties in the satellite model and the external environmental force fields in which it moves. A methodology for the design of a second (additive) adaptive sliding mode controller is developed to guarantee robust trajectory tracking in the presence of these uncertainties. This adaptive control law automatically updates the gain without a priori information about the bounds on the uncertainties involved such that any unknown effects of uncertainties and disturbances that may be time varying are effectively suppressed. The control produces no chattering and the precision with which the trajectory is tracked can be specified by the user. This adaptive control law is developed to track the nominal trajectory designed in the first step so that even in the presence of large initial deviations from the desired formation configuration, the control guarantees robustness throughout the maneuver by keeping the controlled system always in the close vicinity of the sliding surface. This provides a significant advance over currently available approaches that have been proposed in the existing literature.

In brief, the new methodology that is developed in this paper simultaneously achieves three important goals that are useful in real-life applications. They can be summarized as follows:

1. The follower satellite (or satellite formation) is guided to be asymptotically confined to a user-prescribed ‘ball’ of a desired trajectory as though:

    a. any time-varying unknown/uncertain environmental flight disturbances beyond those that are included (on the basis of experience/intuition/etc.) in the system model are no longer present, because the adaptively controlled system follows the nominal trajectory so that it always lies in a user-specified ball, no matter how small, around this nominal trajectory, while the nominal trajectory asymptotically tends to the desired trajectory at a user-specified rate, and
    b. any time-varying unknown/uncertain parameters in the satellite model(s) beyond the best estimates of these parameters used in the system model, are no longer present.
2. The desired trajectory is the optimal trajectory, optimized at each instant of time while minimizing a user-prescribed control cost, for the full nonlinear model in

which no linearizations/approximations are made. This desired trajectory is based on a system model that includes the best available information on the environmental flight uncertainties during the course of the mission and the best available estimates of the uncertain parameters describing the satellite along its trajectory.

3. The upper bounds on the deviations of the environmental uncertainties and the satellite modeling uncertainties from their best estimates used in the system model are *not* required to be known. This is achieved through the development of a new adaptive Lyapunov-based control methodology that guarantees that these uncertainties are compensated for, by having the satellite asymptotically always lie in a 'ball,' no matter how small, of the desired trajectory.

Extensive numerical simulations that consider an uncertain mass of the follower satellite and an uncertain space environment are carried out. Fixed time-step ode4 Runge-Kutta integrators are used to more closely reflect the capabilities of embedded on-board micro-controllers usually employed in real-life satellite maneuvers. The results demonstrate the simplicity, effectiveness, and robustness of the proposed control methodology. They show that the convergence to the desired trajectory to within user-specified error bounds is autonomously attained despite large initial offset errors and significant levels of time-varying uncertainties both in the satellite model and especially in its flight environment. The effects of saturation on the available control force are also simulated. It is shown that precision tracking of the desired configuration trajectory in the face of unknown environmental disturbances as well as satellite modeling uncertainties is still attained despite control thrust saturation that may arise in real-world systems. An alternative approach using this methodology to reduce/prevent control thrust saturation is also investigated and shown to be efficacious. Future work will include the extension of the proposed control methodology to include attitude control and further improvements in the adaptive control technique for faster and even more accurate tracking.

Authors' Contributions H. Cho conceptualized the problem, proposed the main idea, investigated the solution, performed numerical simulations for verification, wrote the original draft, and edited and finalized the manuscript. F. E. Udwadia developed and rigorously investigated the adaptive control, edited, and wrote several parts of the final manuscript. T. Wanichanon supported the investigation of the solution and edited the manuscript.Data AvailabilityNot Applicable.

Compliance with Ethical Standards

Conflicts of Interest/Competing Interests None.

Code Availability Not available.

References

1. Aoude, G.S., How, J.P., Garcia, I.M.: Two-stage path planning approach for designing multiple spacecraft reconfiguration maneuvers. In: Proceedings of the 20th International Symposium on Space Flight Dynamics. Annapolis, USA, September (2007)

2. Clohessy, W.H., Wiltshire, R.S.: Terminal guidance system for satellite rendezvous. J. Aerospace Sci. **27**, 653–658 (1960)
3. Tschauner, J., Hempel, P.: Rendezvous zueinem in elliptischer bahn umlaufenden ziel. Astronautica Acta. **11**, 104–109 (1965)
4. Won, C.H., Ahn, H.S.: Nonlinear orbital dynamic equations and state-dependent Riccati equation control of formation flying satellites. J. Astronaut. Sci. **51**, 433–449 (2003)
5. Wong, H., Kapila, V., Sparks, A.: Adaptive output feedback tracking control of multiple spacecraft. In: Proceedings of the 2001 American control conference, Arlington, USA, June (2001)
6. de Queiroz, M.S., Kapila, V., Yan, Q.: Adaptive nonlinear control of multiple spacecraft formation flying. J. Guid. Control Dynam. **23**, 385–390 (2000)
7. Vignal, P., Pernicka, H.: Low-thrust spacecraft formation keeping. J. Spacecraft Rockets. **43**, 466–475 (2006)
8. Breger, L., How, J.P.: Gauss's variational equation-based dynamics and control for formation flying spacecraft. J. Guid. Control Dynam. **30**, 437–448 (2007)
9. Lim, Y., Jung, Y., Bang, H.: Robust model predictive control for satellite formation keeping with eccentricity/inclination vector separation. Adv. Space Res. **61**, 2661–2672 (2018)
10. Hu, Y.-R., Ng, A.: Robust control of spacecraft formation flying. J. Aerosp. Eng. **20**, 209–214 (2007)
11. Utkin, V.: Sliding Modes in Control and Optimization. Springer, Berlin (1992)
12. Utkin, V., Guldner, J., Shi, J.: Sliding Modes in Electromechanical Systems. Taylor and Francis, London (1999)
13. Yeh, H., Nelson, E., Sparks, A.: Nonlinear tracking control for satellite formations. J. Guid. Control Dynam. **25**, 376–386 (2002)
14. Burton, J.A., Zinober, A.S.: Continuous approximation of variable structure control. Int. J. Syst. Sci. **17**, 875–885 (1986)
15. Massey, T., Shtessel, Y.: Continuous traditional and high-order sliding modes for satellite formation control. J. Guid. Control Dynam. **28**, 826–831 (2005)
16. Udwadia, F.E., Wanichanon, T., Cho, H.: Methodology for satellite formation-keeping in the presence of system uncertainties. J. Guid. Control Dynam. **37**, 1611–1624 (2014)
17. Godard, Kumar, K.D.: Fault tolerant reconfigurable satellite formations using adaptive variable structure techniques. J. Guid. Control Dynam. **33**, 969–984 (2010)
18. Bae, J., Kim, Y.: Adaptive controller design for spacecraft formation flying using sliding mode controller and neural networks. J. Frankl. Inst. **349**, 578–603 (2012)
19. Udwadia, F.E., Kalaba, R.E.: Analytical Dynamics: a New Approach. Cambridge University Press, New York (1996)
20. Koganti, P.B., Udwadia, F.E.: Dynamics and precision control of tumbling multi-body systems. J. Guid. Control Dynam. **40**, 584–602 (2017a)
21. Koganti, P.B., Udwadia, F.E.: Dynamics and precision control of uncertain tumbling multi-body systems. J. Guid. Control Dynam. **40**, 1177–1190 (2017b)
22. Udwadia, F.E.: A new perspective on the tracking control of nonlinear structural and mechanical systems. Proc. R. Soc. London, Ser. A. **459**, 1783–1800 (2003)
23. Udwadia, F.E., Schutte, A.D.: A unified approach to rigid body rotational dynamics and control. Proc. R. Soc. London, Ser. A. **468**, 395–414 (2012)
24. Udwadia, F.E., Wanichanon, T.: Control of uncertain nonlinear multi-body mechanical systems. J. Appl. Mech. **81**, 041020 (2013)
25. Udwadia, F.E., Koganti, P.B.: Dynamics and control of a multi-body planar pendulum. Nonlinear Dynam. **81**, 845–866 (2015)
26. Udwadia, F.E., Koganti, P.B.: Unified approach to modeling and control of rigid multi-body systems. J. Guid. Control Dynam. **39**, 2683–2698 (2016)
27. Cho, H., Yu, A.: New approach to satellite formation-keeping: exact solution to the full nonlinear problem. J. Aerosp. Eng. **22**, 445–455 (2009)
28. Cho, H., Udwadia, F.E.: Explicit solution to the full nonlinear problem for satellite formation-keeping. Acta Astronaut. **67**, 369–387 (2010)
29. Cho, H., Udwadia, F.E.: Explicit control force and torque determination for satellite formation-keeping with attitude requirements. J. Guid. Control Dynam. **36**, 589–605 (2013)
30. Wanichanon, T., Cho, H., Udwadia, F.E.: Satellite formation-keeping using the fundamental equation in the presence of uncertainties in the system. In: Proceedings of AIAA SPACE 2011 Conference & Exposition. Long Beach, USA, September (2011)
31. Vallado, V.A.: Fundamentals of Astrodynamics and Applications, 4th edn. Microcosm Press, El Segundo (2013)

32. Vaddi, S.S., Vadali, S.R., Alfriend, K.T.: Formation flying: accommodating nonlinearity and eccentricity perturbations. J. Guid. Control Dynam. **26**, 214–223 (2003)
33. Gurfil, P., Seidelmann, P.K.: Celestial Mechanics and Astrodynamics: Theory and Practice. Springer, Berlin (2016)
34. Tummala, A.R., Dutta, A.: An overview of cube-satellite propulsion technologies and trends. Aerospace. **4**, 58 (2017)
35. Sabol, C., Burns, R., McLaughlin, C.: Satellite formation flying design and evolution. J. Spacecraft Rockets. **38**, 270–278 (2001)
36. Udwadia, F.E., Kalaba, R.E.: A new perspective on constrained motion. Proc. R. Soc. London, Ser. A. **439**, 407–410 (1992)
37. Baumgarte, J.: Stabilization of constraint and integrals of motion in dynamical systems. Comput. Methods Appl. Mech. Eng. **1**, 1–16 (1972)
38. Udwadia, F.E.: Optimal tracking control of nonlinear dynamical systems. Proc. R. Soc. London, Ser. A. **464**, 2341–2363 (2008)
39. Gronwall, T.H.: Note on the derivatives with respect to a parameter of the solutions of a system of differential equations. Ann. Math. **20**, 292–296 (1919)
40. Hu, Q., Xiao, B.: Adaptive fault tolerant control using integral sliding mode strategy with application to flexible spacecraft. Int. J. Syst. Sci. **44**, 2273–2286 (2013)
41. Mobayen, S.: A novel global sliding mode control based on exponential reaching law for a class of underactuated systems with external disturbances. J. Comput. Nonlinear Dyn. **11**, 021011 (2016)
42. Franklin, G.F., Powell, J.D., Emami-Naeini, A.: Feedback Control of Dynamic Systems, 7th edn. Pearson Higher Education, Upper Saddle River (2015)

Affiliations

Hancheol Cho[1] · **Firdaus E. Udwadia**[2] · **Thanapat Wanichanon**[3]

Firdaus E. Udwadia
feuusc@gmail.com

Thanapat Wanichanon
thanapat.wan@mahidol.edu

[1] Department of Mechanical Engineering, Bradley University, 1501 W Bradley Ave, Peoria, IL 61625, USA

[2] Departments of Aerospace and Mechanical Engineering, Civil and Environmental Engineering, Mathematics, Systems Architecture Engineering, and Information and Operations Management, University of Southern California, 3650 McClintock Ave, Los Angeles, CA 90089, USA

[3] Department of Mechanical Engineering, Mahidol University, 25/25 Phuttamonthon, Phutthamonthon District, Nakorn Pathom 73170, Thailand